A well-conditioned weak coupling of boundary element and high-order finite element methods for time-harmonic electromagnetic scattering by inhomogeneous objects

Ismaïl Badia, Boris Caudron, Xavier Antoine, Christophe Geuzaine

A well-conditioned weak coupling of boundary element and high-order finite element methods for time-harmonic electromagnetic scattering by inhomogeneous objects

Ismaïl BADIA[a,b,c,*], Boris CAUDRON[d], Xavier ANTOINE[b], Christophe GEUZAINE[c]

[a] *Thales Defence Mission Systems France, 2 Avenue Gay-Lussac, 78851 Elancourt cedex, France*
[b] *Université de Lorraine, CNRS, Inria, IECL, F-54000 Nancy, France*
[c] *Université de Liège, Institut Montefiore B28, 4000 Liège, Belgium*
[d] *Thales Defence Mission Systems France, 525 Route des Dolines, Les Bouillides, 06903 Sophia Antipolis, France*

Abstract

The aim of this paper is to propose efficient weak coupling formulations between the boundary element method and the high-order finite element method for solving time-harmonic electromagnetic scattering problems. The approach is based on the use of a non-overlapping domain decomposition method involving optimal transmission operators. The associated transmission conditions are constructed through a localization process based on complex rational Padé approximants of the nonlocal Magnetic-to-Electric operators. Numerical results are presented to validate and analyze the new approach for both homogeneous and inhomogeneous scatterers.

Keywords: Maxwell's equations; time-harmonic scattering; weak coupling; optimized domain decomposition method; high-order finite elements; boundary elements.

Contents

*Corresponding author
Email addresses: ismail.badia@doct.uliege.be (Ismaïl BADIA), boris.caudron@thalesgroup.com (Boris CAUDRON), xavier.antoine@univ-lorraine.fr (Xavier ANTOINE), cgeuzaine@uliege.be (Christophe GEUZAINE)

1. Introduction

The time-harmonic Maxwell equations, which describe the propagation of electromagnetic waves, are essential for a wide range of technological applications as e.g. in antenna and radar design. Numerically solving three-dimensional time-harmonic electromagnetic scattering problems is known to be challenging since it leads to the discretization of a system of partial differential equations set in an unbounded domain. In addition, in the high frequency regime, i.e. when the wavelength λ is small compared to the characteristic size of the scatterer, very fine discretization grids are required to capture the highly oscillatory wave field solution, leading to a huge number of degrees of freedom and associated large size linear systems to solve.

Various approaches can be used to numerically solve time-harmonic electromagnetic scattering problems by a bounded dielectric and inhomogeneous object placed in a homogeneous domain which extends to infinity. Among the most widely used, we can mention the Finite Element Method (FEM) with an Absorbing/Artificial Boundary Condition (ABC) [23] or a Perfectly Matched Layer (PML) [4, 10, 23] to bound the computational domain. This method is well-suited for tackling complex geometrical configurations and heterogeneous media. However, using the FEM for wave problems is known to suffer from the so-called pollution effect [30] related to the accumulation of phase error over the mesh. From a practical point of view, this implies that the mesh size h must be adapted according to the wavenumber $k = 2\pi/\lambda$. A way to reduce the pollution error without refining the mesh is to increase the order of the shape functions involved in the FEM. In addition, solving the large size complex-valued and possibly indefinite linear system associated to the FEM approach, especially in the high-frequency regime, remains computationally challenging. To this end, specifically designed efficient and robust solvers are needed [1, 14, 16, 17, 18, 32, 33, 35, 41]. To avoid the treatment of the exterior domain by the FEM, an alternative approach, called *FEM-BEM coupling*, consists in combining the FEM for the inhomogeneous part of the computational domain with a surface integral equation for the exterior domain, set on the boundary of the scatterer [31], and discretized by the Boundary Element Method (BEM). Although the discretization of an integral equation results in a complex-valued indefinite matrix which is fully populated and expensive to store and solve, advanced compression algorithms like the Fast Multipole Method (FMM) [26] or Hierarchical Matrices (H-Matrices) [7, 20] remedy these drawbacks. A FEM-BEM coupling therefore combines the advantages of both methods.

Standard FEM-BEM techniques consist in combining a surface integral equation for the exterior domain and a volume variational formulation for the interior domain within a single linear system—an approach often called *strong* FEM-BEM coupling (see e.g. [12, 21, 22, 24, 25, 40, 44]). Such direct formulations unfortunately have some major drawbacks that limit their application for solving high-frequency problems. First, strongly coupled methods yield very large size indefinite complex-valued linear systems defined by a matrix with has both sparse and dense parts. Such linear systems are

generally difficult to solve and not adapted to compression algorithms for the nonlocal integral part. Moreover, it is not possible to combine two pre-existing efficient solvers, i.e. one FEM solver for the interior domain and one BEM solver for the exterior domain, to construct a global optimized solver for the coupled formulation. To remedy these drawbacks, alternative *weak* FEM-BEM couplings were recently introduced for the three-dimensional Helmholtz equation that arises in acoustics [3, 6, 9] and for the time-harmonic Maxwell's equations [41]. Non-conformal weak FEM-BEM couplings have also been proposed [32, 43] (e.g. independently generated meshes for different parts of the problem under analysis) but may introduce additional approximation errors. The weak FEM-BEM approach can be interpreted as an optimized Schwarz domain decomposition method (DDM) iterating between the bounded scatterer and the exterior complementary domain until a global convergence criterion is reached. One of the strengths of the weak FEM-BEM approach is that using two pre-existing optimized solvers, one for the BEM and one for the FEM, is direct. Therefore, in the context of an industrial collaboration, using two independently developed solvers could be a considerable advantage. Indeed, for each interior/exterior electromagnetic subproblem, different partners (e.g. aircraft/antenna designers) can exchange minimal information at the transmitting boundary between the two subdomains to solve the global electromagnetic problem without sharing their simulation codes and the details of the models.

To design an efficient weak FEM-BEM coupling, it is crucial to consider a fast converging Schwarz DDM algorithm. For wave propagation problems, and most particularly in the high-frequency regime, the key computational ingredient in the implementation of an efficient and robust converging DDM is to design well-suited transmission conditions between the interfaces of the subdomains. In electromagnetism, the optimal transmission condition is defined through the Magnetic-to-Electric (MtE) map that links the magnetic and the electric surface currents at the interface of the subdomains [8]. From a computational point of view, the numerical evaluation of this operator is nevertheless costly since the MtE operator is a nonlocal pseudodifferential operator. This is the reason why Schwarz DDM with optimized local transmitting boundary conditions were proposed in the literature [1, 13, 14, 16, 17, 35]. In the context of the weak FEM-BEM coupling, it was shown in [8, 9] that a fast convergence can be expected when using the Padé expansion of a square-root operator which approximates the nonlocal Dirichlet-to-Neumann (DtN) operator, where the DtN map plays the role of the MtE operator but for acoustics. The aim of the paper is to present the extension and some improvements of the weak FEM-BEM coupling method to the electromagnetic scattering problem by an inhomogeneous scatterer by using high-order finite element methods. This new weak FEM-BEM coupling formulation is shown to exhibit a convergence rate that is only slightly dependent on the wavenumber k, the mesh refinement h and the contrast between the two subdomains. Note that for homogeneous obstacles one can use a weak BEM-BEM coupling formulation.

The article is organized as follows. Section 2 describes the electromagnetic transmission-scattering problem. In Section 3, we present the weak coupling approach. Section 4 is devoted to the construction of approximate nonlocal MtE surface operators. Section 5 provides the formulations for solving the weak coupling and associated subproblems. Section 6 details the finite element implementation of the weak coupling. Numerical results for three-dimensional electromagnetic scattering problems by homogeneous and inhomogeneous obstacles are presented in Section 7. We finally conclude in Section 8.

2. The electromagnetic transmission-scattering problem

Let Ω_- be a bounded scatterer in $\mathbb{R}^3$ with smooth closed boundary $\Gamma := \partial\Omega_-$. The exterior unbounded domain of propagation is defined by $\Omega_+ := \mathbb{R}^3 \setminus \overline{\Omega_-}$. We consider an incident electromagnetic plane wave $(\mathbf{E_{inc}};\mathbf{H_{inc}})$ propagating in the unbounded domain Ω_+ and satisfying the exterior time-harmonic Maxwell's equations

$$\left\{ \begin{array}{rcl} \mathbf{curl}\,\mathbf{E_{inc}} - \imath k_+ \mathcal{Z}_+ \mathbf{H_{inc}} & = & 0 \\ \mathbf{curl}\,\mathbf{H_{inc}} + \imath k_+ \mathcal{Z}_+^{-1} \mathbf{E_{inc}} & = & 0 \end{array} \right. \quad \text{in } \Omega_+.$$

The object generates an outgoing scattered wave $(\mathbf{E_{sc}};\mathbf{H_{sc}})$. Let us define $(\mathbf{E}_+;\mathbf{H}_+) = (\mathbf{E_{inc}};\mathbf{H_{inc}}) + (\mathbf{E_{sc}};\mathbf{H_{sc}})$ as the total electromagnetic field in the exterior domain Ω_+. Then, our goal is to solve the following boundary-value problem: find the wave field $\mathbf{E} \in \mathbf{H}(\mathbf{curl},\Omega_-) \cup \mathbf{H}_{\rm loc}(\mathbf{curl},\overline{\Omega_+})$[1] solution of the following electromagnetic transmission-scattering problem

$$\mathbf{curl}\left(\frac{1}{k_-\mathcal{Z}_-}\mathbf{curl}\,\mathbf{E}\right) - k_-\mathcal{Z}_-^{-1}\mathbf{E} = \mathbf{0}, \quad \text{in } \Omega_-, \tag{2.1a}$$

$$\mathbf{curl}\,\mathbf{curl}\,\mathbf{E} - k_+^2\mathbf{E} = \mathbf{0}, \quad \text{in } \Omega_+, \tag{2.1b}$$

$$\frac{1}{\imath k_+}\mathbf{curl}\,\mathbf{E_{sc}} \times \frac{\mathbf{x}}{\|\mathbf{x}\|} - \mathbf{E_{sc}} = \underset{r\to+\infty}{\mathcal{O}}(r^{-2}), \tag{2.1c}$$

$$\boldsymbol{\gamma}_t^-\mathbf{E} = \boldsymbol{\gamma}_t^+\mathbf{E}, \quad \text{on } \Gamma, \tag{2.1d}$$

$$\boldsymbol{\gamma}_t^-\left(\frac{1}{k_-\mathcal{Z}_-}\mathbf{curl}\,\mathbf{E}\right) = \frac{1}{k_+\mathcal{Z}_+}\boldsymbol{\gamma}_t^+\left(\mathbf{curl}\,\mathbf{E}\right), \quad \text{on } \Gamma. \tag{2.1e}$$

In the above equations, $k_\pm := \omega\sqrt{\varepsilon_\pm\mu_\pm}$ and $\mathcal{Z}_\pm := \sqrt{\frac{\mu_\pm}{\varepsilon_\pm}}$ denote respectively the wavenumbers and the impedances associated with $\Omega_\pm$, where ω is the angular frequency, and $\varepsilon_\pm$ and $\mu_\pm$ stand for the permittivities and permeabilities in $\Omega_\pm$. In practice, the exterior domain is made of air so that $\mathcal{Z}_+$ corresponds to the free space impedance $\mathcal{Z}_0$. To include the case of heterogeneous dielectric materials, k_- and $\mathcal{Z}_-$ can be space-dependent functions of $\mathbf{x} \in \mathbb{R}^3$. We introduce a contrast parameter $\delta \in \mathbb{R}$ such as, in case of homogeneous scatterers and $\mu_+ = \mu_-$, $k_- = \delta k_+$ and $\mathcal{Z}_- = \frac{\mathcal{Z}_+}{\delta}$. The curl operator of a vector field $\mathbf{u} \in \mathbb{R}^3$ is denoted by $\mathbf{curl}\,\mathbf{u}$. The unit imaginary number is $\imath = \sqrt{-1}$. The notation $\mathbf{u}\times\mathbf{v}$ designates the cross product and $\mathbf{u}\cdot\overline{\mathbf{v}}$ the inner product between two complex valued vector fields $\mathbf{u}$ and $\mathbf{v}$ in $\mathbb{C}^3$, where $\overline{\mathbf{v}}$ is the complex conjugate of $\mathbf{v}$. The associated norm is $\|\mathbf{x}\| := \sqrt{\mathbf{x}\cdot\overline{\mathbf{x}}}$. Equation (2.1c) is the Silver-Müller radiation condition at infinity with $\mathbf{x} = r\boldsymbol{\sigma} \in \mathbb{R}^3$, $r := \|\mathbf{x}\|$ the radial coordinate and $\boldsymbol{\sigma}$ the unit radial vector. Finally, the transmission conditions (2.1d) and (2.1e) respectively express the tangential continuity of the total electric and magnetic fields through Γ. These transmission conditions involve the tangential trace operators $\boldsymbol{\gamma}_t^\pm$ defined by

$$\begin{array}{rcccc} \boldsymbol{\gamma}_t^\pm & : & \mathbf{H}(\mathbf{curl},\Omega_-) \cup \mathbf{H}_{\rm loc}(\mathbf{curl},\overline{\Omega_+}) & \to & \mathbf{H}_t^{-\frac{1}{2}}(\mathrm{div}_\Gamma,\Gamma) \\ & & \mathbf{u} & \mapsto & \mathbf{u}_{\pm|\Gamma}\times\mathbf{n} \end{array},$$

with $\mathbf{n}$ the outward-pointing unit normal vector of Ω_- on Γ and $\mathbf{H}_t^{-\frac{1}{2}}(\mathrm{div}_\Gamma,\Gamma) = \{\mathbf{v} \in \mathbf{H}_t^{-\frac{1}{2}}(\Gamma) : \mathrm{div}_\Gamma\mathbf{u} \in \mathrm{H}^{-\frac{1}{2}}(\Gamma)\}$, where the surface divergence operator div_Γ [31] has to be taken in the distributional sense. The space $\mathbf{H}_t^{-\frac{1}{2}}(\Gamma)$ designates the dual of the Hilbert space $\mathbf{H}_t^{\frac{1}{2}}(\Gamma) = \{\mathbf{u} \in \mathbf{H}^{\frac{1}{2}}(\Gamma) :$

[1] $\mathbf{H}(\mathbf{curl},\Omega_-) = \{\mathbf{v} \in \mathbf{L}^2(\Omega_-) : \mathbf{curl}\,\mathbf{v} \in \mathbf{L}^2(\Omega_-)\}$; $\mathbf{H}_{\rm loc}(\mathbf{curl},\overline{\Omega_+}) = \{\mathbf{v} \in \mathbf{H}(\mathbf{curl},\mathcal{B}\setminus\overline{\Omega_-}) :$ for every open ball $\mathcal{B}$ containing Ω_- in its interior$\}$.

$\mathbf{u}\cdot\mathbf{n} = 0\}$. Provided that k_- and $\mathcal{Z}_-$ are piecewise smooth and bounded away from zero everywhere in Ω_-, the transmission-scattering problem (2.1) has a unique solution [21]. An illustration of the problem is given in Fig. 1.

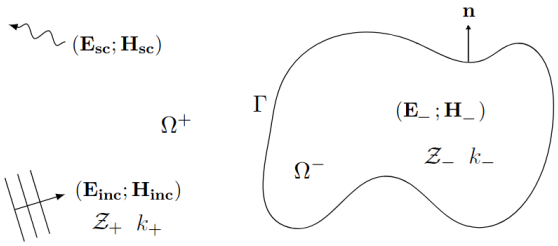

Figure 1: The electromagnetic transmission-scattering problem.

3. The weak coupling approach

A classical way to solve (2.1) is to couple a surface integral formulation for the exterior problem and a variational volume formulation for the interior domain within a single equation, leading to a strong FEM-BEM coupling. As noted in the introduction, these methods have however several drawbacks. We therefore rather consider a weak coupling approach. This method is essentially a non-overlapping Schwarz DDM based on the following decomposition of $\mathbb{R}^3$: $\mathbb{R}^3 = \Omega_- \cup \Omega_+ \cup \Gamma$. The Schwarz DDM is solved in practice *via* an iterative method such as GMRES [37, 38]. The key point to get a fast converging DDM is to design optimized transmission conditions at the interface Γ. For the time-harmonic Maxwell equations, Després first proposed in [13] to use a simple impedance boundary operator to obtain a converging algorithm. Several other local transmission conditions were later derived (see e.g. [1, 13, 14, 15, 16, 17, 33, 35]). Similarly, the well-conditioned weak coupling algorithm requires the use of adapted interface conditions. In this work, we will use nonlocal MtE maps and their localization through Padé approximants [8, 17] to achieve fast convergence.

3.1. Reformulating the problem

The first step of the method consists in reformulating the transmission conditions (2.1d)-(2.1e). Let us introduce the following two transmission operators

$$\mathbf{T}_- : \mathbf{H}_t^{-\frac{1}{2}}(\mathrm{div}_\Gamma,\Gamma) \to \mathbf{H}_t^{-\frac{1}{2}}(\mathrm{div}_\Gamma,\Gamma),\ \ \mathbf{T}_+ : \mathbf{H}_t^{-\frac{1}{2}}(\mathrm{div}_\Gamma,\Gamma) \to \mathbf{H}_t^{-\frac{1}{2}}(\mathrm{div}_\Gamma,\Gamma). \tag{3.1}$$

Since we work with total fields, $\mathbf{T}_\pm$ are affine operators. We assume that $\mathbf{T}_- + \mathbf{T}_+$ is injective so that the transmission conditions (2.1d)-(2.1e) are equivalent to the following transmission conditions

$$\left\{\begin{array}{rcl} \boldsymbol{\gamma}_t^- \mathbf{H} + \mathbf{T}_- \boldsymbol{\gamma}_t^- \mathbf{E} & = & \boldsymbol{\gamma}_t^+ \mathbf{H} + \mathbf{T}_- \boldsymbol{\gamma}_t^+ \mathbf{E} \\ \boldsymbol{\gamma}_t^+ \mathbf{H} - \mathbf{T}_+ \boldsymbol{\gamma}_t^+ \mathbf{E} & = & \boldsymbol{\gamma}_t^- \mathbf{H} - \mathbf{T}_+ \boldsymbol{\gamma}_t^- \mathbf{E} \end{array}\right. . \tag{3.2}$$

DDMs are usually constructed by assuming that $\mathbf{T}_+ = \mathbf{T}_-$ (see e.g. [17]). Here, however, we consider that they can be different for more generality and flexibility. Then, we introduce the following trace operators

$$\forall (\mathbf{E};\mathbf{H}) \in [\mathbf{H}(\mathbf{curl},\Omega_-) \cup \mathbf{H}_{\mathrm{loc}}(\mathbf{curl},\overline{\Omega_+})]^2,\ \ \mathbf{B}_\pm(\mathbf{E};\mathbf{H}) = \boldsymbol{\gamma}_t^\pm \mathbf{H} \mp \mathbf{T}_\pm \boldsymbol{\gamma}_t^\pm \mathbf{E},$$

from which we define the unknowns of the weak coupling

$$\mathbf{g}_- = \mathbf{B}_-(\mathbf{E};\mathbf{H}),\ \mathbf{g}_+ = \mathbf{B}_+(\mathbf{E};\mathbf{H}). \tag{3.3}$$

Note that by definition of the unknowns of the weak coupling (3.3), it follows that $\mathbf{g}_\pm \neq \mathbf{0}$. Finally, we still need to introduce the affine resolution operators $\mathbf{R}_-$ and $\mathbf{R}_+$ as: $\forall \mathbf{g} \in \mathbf{H}_t^{-\frac{1}{2}}(\mathrm{div}_\Gamma, \Gamma)$, $\mathbf{R}_\pm \mathbf{g} = \boldsymbol{\gamma}_t^\pm \mathbf{E}_\pm$, where the fields $(\mathbf{E}_-;\mathbf{H}_-) \in \mathbf{H}(\mathbf{curl}, \Omega_-)^2$ and $(\mathbf{E}_+;\mathbf{H}_+) \in \mathbf{H}_{\mathrm{loc}}(\mathbf{curl}, \overline{\Omega_+})^2$ are the solutions of the respective boundary-value problems

$$\left\{\begin{array}{lcl} \mathbf{curl}\ \mathbf{E}_- - \imath k_- \mathcal{Z}_- \mathbf{H}_- & = & \mathbf{0} \ \text{ in } \ \Omega_- \\ \mathbf{curl}\ \mathbf{H}_- + \imath k_- \mathcal{Z}_-^{-1} \mathbf{E}_- & = & \mathbf{0} \ \text{ in } \ \Omega_- \\ \mathbf{B}_-(\mathbf{E}_-;\mathbf{H}_-) = \mathbf{g} \ \text{ on } \ \Gamma & & \end{array}\right. , \tag{3.4}$$

and

$$\left\{\begin{array}{lcl} \mathbf{curl}\ \mathbf{E}_+ - \imath k_+ \mathcal{Z}_+ \mathbf{H}_+ & = & \mathbf{0} \ \text{ in } \ \Omega_+ \\ \mathbf{curl}\ \mathbf{H}_+ + \imath k_+ \mathcal{Z}_+^{-1} \mathbf{E}_+ & = & \mathbf{0} \ \text{ in } \ \Omega_+ \\ \mathcal{Z}_+ \mathbf{H_{sc}} \times \frac{\mathbf{x}}{||\mathbf{x}||} - \mathbf{E_{sc}} & = & \underset{r\to+\infty}{\mathcal{O}}(r^{-2}) \\ \mathbf{B}_+(\mathbf{E}_+;\mathbf{H}_+) = \mathbf{g} \ \text{ on } \ \Gamma & & \end{array}\right. . \tag{3.5}$$

The subproblems (3.4) and (3.5) are associated with the DDM for the weak coupling. Their well-posedness depends on the choice of the transmission operators. We assume here that both problems (3.4) and (3.5) are well-posed so that the resolution operators are correctly defined. We can now introduce the weak coupling formulation of the transmission-scattering problem (2.1).

Proposition 3.1. *The electromagnetic field $(\boldsymbol{E};\boldsymbol{H})$ is the solution of the transmission-scattering problem (2.1) if and only if $\boldsymbol{g}_-$ and $\boldsymbol{g}_+$ are solutions to*

$$(\boldsymbol{Id} - \boldsymbol{\mathcal{S}}_\pi) \begin{pmatrix} \boldsymbol{g}_- \\ \boldsymbol{g}_+ \end{pmatrix} = \begin{pmatrix} \boldsymbol{0} \\ \boldsymbol{0} \end{pmatrix}, \tag{3.6}$$

the operator $\boldsymbol{Id} - \boldsymbol{\mathcal{S}_\pi}$ being defined by

$$\boldsymbol{Id} - \boldsymbol{\mathcal{S}_\pi} = \begin{pmatrix} \boldsymbol{Id} & -\boldsymbol{S}_+ \\ -\boldsymbol{S}_- & \boldsymbol{Id} \end{pmatrix},$$

with $\boldsymbol{S}_\pm = \boldsymbol{Id} \pm (\boldsymbol{T}_- + \boldsymbol{T}_+)\boldsymbol{R}_\pm$.

Proof. We start by rewriting the transmission conditions (3.2) as

$$\mathbf{B}_-(\mathbf{E},\mathbf{H}) = \mathbf{B}_+(\mathbf{E},\mathbf{H}) + (\mathbf{T}_- + \mathbf{T}_+)\boldsymbol{\gamma}_t^+ \mathbf{E},$$

$$\mathbf{B}_+(\mathbf{E},\mathbf{H}) = \mathbf{B}_-(\mathbf{E},\mathbf{H}) - (\mathbf{T}_- + \mathbf{T}_+)\boldsymbol{\gamma}_t^- \mathbf{E}.$$

Since the field $(\mathbf{E};\mathbf{H})$ is solution of (3.4) and (3.5), we deduce that

$$\mathbf{R}_\pm \mathbf{g} = \boldsymbol{\gamma}_t^\pm \mathbf{E},$$

and obtain (3.6). Finally to prove the equivalence, it is sufficient to check that the transmission conditions (3.2) are satisfied, which can be easily proved. ∎

In a domain decomposition setting, let us remark that an iterative Jacobi algorithm [37] for solving (3.6) involves at iteration $n+1$ the resolution of the following subproblems

$$\left\{\begin{array}{lcl} \mathbf{curl}\,\mathbf{E}_-^{n+1} - \imath k_- \mathcal{Z}_- \mathbf{H}_-^{n+1} &=& \mathbf{0} \ \text{ in } \ \Omega_- \\ \mathbf{curl}\,\mathbf{H}_-^{n+1} + \imath k_- \mathcal{Z}_-^{-1} \mathbf{E}_-^{n+1} &=& \mathbf{0} \ \text{ in } \ \Omega_- \\ \mathbf{B}_-(\mathbf{E}_-^{n+1}; \mathbf{H}_-^{n+1}) = \mathbf{g}_-^n & & \end{array}\right. , \tag{3.7}$$

and

$$\left\{\begin{array}{lcl} \mathbf{curl}\,\mathbf{E}_+^{n+1} - \imath k_+ \mathcal{Z}_+ \mathbf{H}_+^{n+1} &=& \mathbf{0} \ \text{ in } \ \Omega_+ \\ \mathbf{curl}\,\mathbf{H}_+^{n+1} + \imath k_+ \mathcal{Z}_+^{-1} \mathbf{E}_+^{n+1} &=& \mathbf{0} \ \text{ in } \ \Omega_+ \\ \mathcal{Z}_+ \mathbf{H}_{\mathbf{sc}}^{n+1} \times \frac{\mathbf{x}}{||\mathbf{x}||} - \mathbf{E}_{\mathbf{sc}}^{n+1} &=& \underset{r\to+\infty}{\mathcal{O}}(r^{-2}) \\ \mathbf{B}_+(\mathbf{E}_+^{n+1}; \mathbf{H}_+^{n+1}) = \mathbf{g}_+^n & & \end{array}\right. , \tag{3.8}$$

and finally the updating of the interface unknowns according to

$$\begin{pmatrix} \mathbf{g}_-^{n+1} \\ \mathbf{g}_+^{n+1} \end{pmatrix} = \boldsymbol{\mathcal{S}}_\pi \begin{pmatrix} \mathbf{g}_-^{n} \\ \mathbf{g}_+^{n} \end{pmatrix}. \tag{3.9}$$

This is equivalent to the following classical Schwarz algorithm

$$\left\{\begin{array}{lcl} \mathbf{curl}\,\mathbf{E}^{n+1} - \imath k_\pm \mathcal{Z}_\pm \mathbf{H}^{n+1} &=& \mathbf{0} \ \text{ in } \ \Omega_\pm \\ \mathbf{curl}\,\mathbf{H}^{n+1} + \imath k_\pm \mathcal{Z}_\pm^{-1} \mathbf{E}^{n+1} &=& \mathbf{0} \ \text{ in } \ \Omega_\pm \\ \mathcal{Z}_+ \mathbf{H}_{\mathbf{sc}}^{n+1} \times \frac{\mathbf{x}}{||\mathbf{x}||} - \mathbf{E}_{\mathbf{sc}}^{n+1} &=& \underset{r\to+\infty}{\mathcal{O}}(r^{-2}) \\ \gamma_t^- \mathbf{H}^{n+1} + \mathbf{T}_- \gamma_t^- \mathbf{E}^{n+1} = \gamma_t^+ \mathbf{H}^n + \mathbf{T}_- \gamma_t^+ \mathbf{E}^n & & \\ \gamma_t^+ \mathbf{H}^{n+1} - \mathbf{T}_+ \gamma_t^+ \mathbf{E}^{n+1} = \gamma_t^- \mathbf{H}^n - \mathbf{T}_+ \gamma_t^- \mathbf{E}^n & & \end{array}\right. .$$

In (3.7) and (3.8), we can interpret $\mathbf{g}_-^n$ and $\mathbf{g}_+^n$ as some exchanged information from Ω_+ to Ω_- and from Ω_- to Ω_+.

3.2. Optimal transmission operators

The weak coupling (3.6) is not suitable for a direct resolution. Indeed, the operator $\mathbf{Id} - \boldsymbol{\mathcal{S}}_\pi$ is defined implicitly from the resolution operators $\mathbf{R}_+$ and $\mathbf{R}_-$, which correspond, at the discrete level, to solving (3.4) and (3.5), respectively. In this work, the final weak coupling linear system is solved *via* an iterative Krylov subspace method (GMRES) [37, 38].

The convergence of the weak coupling is fundamentally related to the choice of the transmission operators $\mathbf{T}_\pm$. To this end, let us introduce the affine nonlocal MtE operators $\boldsymbol{\Lambda}_{\pm,k_\pm,\mathcal{Z}_\pm}$ defined by

$$\begin{array}{rccc} \boldsymbol{\Lambda}_{\pm,k_\pm,\mathcal{Z}_\pm} \ : & \mathbf{H}_t^{-\frac{1}{2}}(\mathrm{div}_\Gamma,\Gamma) & \to & \mathbf{H}_t^{-\frac{1}{2}}(\mathrm{div}_\Gamma,\Gamma) \\ & \boldsymbol{\gamma_t}^{\pm}\mathbf{E} & \mapsto & \boldsymbol{\gamma_t}^{\pm}\mathbf{H} \end{array} .$$

By rewriting (3.3), the MtE, transmission and resolution operators are linked by

$$(\boldsymbol{\Lambda}_{-,k_-,\mathcal{Z}_-} + \mathbf{T}_-)\mathbf{R}_- = \mathbf{Id}, \quad (\boldsymbol{\Lambda}_{+,k_+,\mathcal{Z}_+} - \mathbf{T}_+)\mathbf{R}_+ = \mathbf{Id}.$$

Let us now consider the following important proposition.

Proposition 3.2. *The optimal choice of the transmission operators for the weak coupling (3.6) is given as*

$$\boldsymbol{T}_- = -\boldsymbol{\Lambda}_{+,k_+,\mathcal{Z}_+} \Rightarrow \boldsymbol{S}_+ = \boldsymbol{0} \quad , \quad \boldsymbol{T}_+ = \boldsymbol{\Lambda}_{-,k_-,\mathcal{Z}_-} \Rightarrow \boldsymbol{S}_- = \boldsymbol{0}. \tag{3.10}$$

A direct consequence of this result is that $\mathbf{S}_\pi$ is null when using the MtE operators as transmission operators, leading to a trivial resolution of the weak coupling (3.6). In addition, if only one of the transmission operators $\mathbf{T}_\pm$ is optimal, i.e. one of the two conditions (3.10) holds, then the linear part of $\mathbf{S}_\pi$ is nilpotent and its spectrum is therefore reduced to $\{0\}$. Therefore, the linear part of $\mathbf{Id} - \mathbf{S}_\pi$ is characterized by an eigenvalue clustering on $(1, 0)$ in the complex plane, leading to a fast convergence of the GMRES used to solve the weak coupling. The MtE operators are *a priori* nonlocal operators that lead to high computational costs. To get a reduced evaluation cost for the weak coupling procedure, it is highly desirable to rather consider localized approximations of the MtE operators. Such accurate representations are available in the literature for the exterior MtE operator $\mathbf{\Lambda}_{+,k_+,\mathcal{Z}_+}$ (see Section 4). This can be understood by the fact that the solution to the exterior problem is spatially localized at least for convex domains, in particular in the high-frequency regime, where constructive methods are then possible. Therefore, it is reasonable to get access to an accurate computation of $\mathbf{T}_- = -\mathbf{\Lambda}_{+,k_+,\mathcal{Z}_+}$, which then leads to an almost nilpotent linear part of $\mathbf{S}_\pi$. Building an accurate approximation of $\mathbf{T}_+ = \mathbf{\Lambda}_{-,k_-,\mathcal{Z}_-}$ is more difficult, and can even be impossible by localized operators due to the presence of multiply bouncing internal waves in Ω_- corresponding to complex nonlocal interactions. Since we can get an accurate representation of $\mathbf{T}_-$ and almost a nilpotent linear part of $\mathbf{S}_\pi$, a rough approximation of $\mathbf{\Lambda}_{-,k_-,\mathcal{Z}_-}$ to get $\mathbf{T}_+$, e.g. by a constant, may seem to be sufficient. However, this can sometimes not be the case as it was observed in [9] for the acoustic case and here for the electromagnetic case (see Section 7) where an increase of GMRES iterations can be observed at some specific frequencies, while leading nevertheless to a converging weak coupling procedure with a correct solution. This drawback is accentuated when the contrast between the exterior and interior domains is high. An alternative choice that appears first as less natural for a two domain decomposition is to rather extend in a fictive way the exterior problem into Ω_- by setting $\mathbf{T}_+ = -\mathbf{\Lambda}_{+,k_+,\mathcal{Z}_+} = \mathbf{T}_-$. This leads to improved convergence at these specific frequencies, even with a rough approximation of $\mathbf{T}_+$ by a constant (and then $\mathbf{T}_+ \neq \mathbf{T}_-$ when localized). We will see in Section 7 that this improvement is important most particularly for the high contrast case.

Finally, let us remark that an alternative choice of the operators $\mathbf{T}_\pm$ could have been made to optimize the resolution of the subproblems (3.4) and (3.5), e.g. to get well-conditioned integral equation formulations [8]. These optimal operators are different from those of the weak coupling. Since our main objective is to precondition the weak coupling (3.6), we only consider here the adapted transmission operators (3.10).

4. Approximations of the MtE maps

The MtE operators $\mathbf{\Lambda}_{\pm,k,\mathcal{Z}}$ are usually not available for a general shape Γ. Let us note that for a magnetic current $\mathbf{m}$, we can write $\mathbf{m} = \widetilde{\mathbf{m}} + \mathbf{m_{inc}}$ where $\mathbf{m_{inc}}$ is the contribution of the incident field ($\mathbf{m_{inc}} = \mathbf{0}$ if there is none) and $\widetilde{\mathbf{m}} = \mathbf{m} - \mathbf{m_{inc}}$. In the following, we propose to decompose the affine operators $\mathbf{\Lambda}_{\pm,k,\mathcal{Z}}$ such that $\forall \mathbf{m}$, $\mathbf{\Lambda}_{\pm,k,\mathcal{Z}}(\mathbf{m}) = \widetilde{\mathbf{\Lambda}_{\pm,k,\mathcal{Z}}}(\widetilde{\mathbf{m}}) + \mathbf{\Lambda}^{\mathbf{inc}}_{\pm,k,\mathcal{Z}}$ where $\widetilde{\mathbf{\Lambda}_{\pm,k,\mathcal{Z}}}$ are linear operators and $\mathbf{\Lambda}^{\mathbf{inc}}_{\pm,k,\mathcal{Z}} = \widetilde{\mathbf{\Lambda}_{\pm,k,\mathcal{Z}}}(\mathbf{m_{inc}})$ (for the contribution of the incident field).

4.1. Nonlocal approximations of the linear part of the MtE operators

Let us assume that Γ is a general smooth convex surface. Based on microlocal analysis [15], we can build the following nonlocal surface approximations $\mathbf{\Lambda}^{\mathrm{sq}}_{\pm,k,\mathcal{Z}}$ of $\widetilde{\mathbf{\Lambda}_{\pm,k,\mathcal{Z}}}$

$$\mathbf{\Lambda}^{\mathrm{sq}}_{\pm,k,\mathcal{Z}} = \mp\frac{1}{\mathcal{Z}}(\mathbf{Id} + \boldsymbol{\nabla}_\Gamma(\frac{1}{k_\epsilon^2}\mathrm{div}_\Gamma) - \mathbf{curl}_\Gamma(\frac{1}{k_\epsilon^2}\mathrm{curl}_\Gamma))^{-\frac{1}{2}}(\mathbf{Id} - \mathbf{curl}_\Gamma(\frac{1}{k_\epsilon^2}\mathrm{curl}_\Gamma))(\mathbf{Id} \times \mathbf{n}), \qquad (4.1)$$

with $k_\epsilon = k + \iota\epsilon$. The accuracy of (4.1) used as an OSRC [15] depends crucially on the choice of the regularization parameter ϵ. A well-suited value is $\epsilon = 0.39 k^{\frac{1}{3}} \mathcal{H}^{\frac{2}{3}}$, with $\mathcal{H}$ the local mean curvature. Since the operators $\mathbf{\Lambda}^{\mathrm{sq}}_{\pm,k_\pm,\mathcal{Z}_\pm}$ are used as preconditioners for the weak coupling procedure, we can simplify this expression by replacing $\mathcal{H}$ by the inverse of the radius of the circumscribed sphere to Ω_-. The operators $\boldsymbol{\nabla}_\Gamma$, $\mathbf{curl}_\Gamma$ and curl_Γ designate the surface gradient, the vector and scalar surface curl operators [31], respectively. If k and $\mathcal{Z}$ are space-dependent functions, we will formally extend (4.1) which can be justified thanks to the theory of pseudodifferential operators and the associated microlocal analysis techniques (see e.g. some examples in [27] for scalar wave equation). It is worth noting that the theory of pseudodifferential operators is developed by assuming that the surface is smooth. By weakening the regularity, for example near a corner, the approximations (4.1) may lose some accuracy since they are not rigorously valid. However, again because they numerically act as preconditioners for the weak coupling algorithms, this has a limited impact in the global convergence of the iterative scheme (e.g. GMRES). It would however be very interesting to improve the convergence of the current method by carefully including the corner effects [29].

In practice, $\mathbf{\Lambda}^{\mathrm{sq}}_{+,k_+,\mathcal{Z}_+}$ provides a suitable approximation of $\widetilde{\mathbf{\Lambda}_{+,k_+,\mathcal{Z}_+}}$, and then the linear part of $\mathbf{T}_-$ for the weak coupling, in particular for large wavenumbers k_+. However, since $\widetilde{\mathbf{\Lambda}_{-,k_-,\mathcal{Z}_-}}$ is usually a strongly nonlocal operator, its approximation by $\mathbf{\Lambda}^{\mathrm{sq}}_{-,k_-,\mathcal{Z}_-}$ is relatively limited. For k_- and $\mathcal{Z}_-$ constant, a possible alternative would be to use an integral approximation (see e.g. Section 5.3.3, pages 133-134 in [8]). However, this choice may appear as costly in practice. Since we are already considering a suitable approximation of $\mathbf{T}_-$, as mentioned before, a rough approximation of $\mathbf{T}_+$ is however sufficient because the linear part of $\mathbf{S}_\pi$ is almost nilpotent. We will see in Section 7 that an approximation of the linear part of $\mathbf{T}_+$ by a brute force approximation of $-\mathbf{\Lambda}^{\mathrm{sq}}_{+,k_+,\mathcal{Z}_+}$ based on a constant leads to very satisfactory convergence results.

4.2. Localization of the linear part of the MtE operators

The approximations (4.1) involve nonlocal pseudodifferential operators that are computationally expensive to evaluate directly and lead to full discrete matrix representations (when they can be computed). A practical approach is to further use localized approximations of the inverse square-root symbol. The simplest approximation of $\mathbf{\Lambda}^{\mathrm{sq}}_{+,k,\mathcal{Z}}$ and $\mathbf{\Lambda}^{\mathrm{sq}}_{-,k,\mathcal{Z}}$ is to use a Taylor expansion in $1/k$ truncated at the zeroth-order term following

$$\mathbf{\Lambda}^{0}_{\pm,k,\mathcal{Z}} = \mp \frac{1}{\mathcal{Z}} (\mathbf{Id} \times \mathbf{n}). \tag{4.2}$$

More accurate local approximations of $\mathbf{\Lambda}^{\mathrm{sq}}_{\pm,k,\mathcal{Z}}$, leading to Padé-localized square-root approximations that we denote by $\mathbf{\Lambda}^{\mathrm{sq},N_p,\theta_p}_{\pm,k,\mathcal{Z}}$, were proposed in [15]. To this end, let us introduce the rational Padé approximation of order N_p of the square-root function [28], with θ_p-rotation of the branch-cut: $\forall z \in \mathbb{C},\ \mathcal{R}(z) > -1,\ \forall j \in \{1; ...; N_p\}, z \neq -B_j^{-1}$,

$$(1+z)^{\frac{1}{2}} \approx e^{\iota \frac{\theta_p}{2}} R_{N_p}((1+z)e^{-\iota\theta_p} - 1) = C_0 + \sum_{\ell=1}^{N_p} \frac{A_\ell z}{1 + B_\ell z}, \tag{4.3}$$

where R_{N_p} is the usual real-valued Padé approximation of order N_p

$$R_{N_p} = 1 + \sum_{\ell=1}^{N_p} \frac{a_\ell z}{1 + b_\ell z} \text{ with } a_\ell = \frac{2}{2N_p+1} \sin^2\left(\frac{\ell\pi}{2N_p+1}\right) \text{ and } b_\ell = \cos^2\left(\frac{\ell\pi}{2N_p+1}\right).$$

The angle of rotation θ_p is a free parameter that is fixed for the numerical simulations and

$$C_0 = e^{\iota\frac{\theta_p}{2}} R_{N_p}(e^{-\iota\theta_p} - 1),\ A_\ell = \frac{e^{-\iota\frac{\theta_p}{2}} a_\ell}{(1 + b_\ell(e^{-\iota\theta} - 1))^2},\ B_\ell = \frac{e^{-\iota\theta_p} b_\ell}{1 + b_\ell(e^{-\iota\theta} - 1)}.$$

Formally, considering that $\boldsymbol{\mathcal{J}} = \boldsymbol{\nabla}_\Gamma(\frac{1}{k_\epsilon^2}\mathrm{div}_\Gamma) - \mathbf{curl}_\Gamma(\frac{1}{k_\epsilon^2}\mathrm{curl}_\Gamma)$, the Padé approximation (4.3) leads to the following approximate linear operators $\boldsymbol{\Lambda}^{\mathrm{sq},N_p,\theta_p}_{\pm,k,\mathcal{Z}}$ of $\boldsymbol{\Lambda}^{\mathrm{sq}}_{\pm,k,\mathcal{Z}}$

$$\boldsymbol{\Lambda}^{\mathrm{sq},N_p,\theta_p}_{\pm,k,\mathcal{Z}} = \mp\frac{1}{\mathcal{Z}}\left(C_0\mathbf{Id} + \sum_{\ell=1}^{N_p} A_\ell \boldsymbol{\mathcal{J}}(\mathbf{Id} + B_\ell\boldsymbol{\mathcal{J}})^{-\mathbf{1}}\right)^{-1}\left(\mathbf{Id} - \mathbf{curl}_\Gamma(\frac{1}{k_\epsilon^2}\mathrm{curl}_\Gamma)\right)(\mathbf{Id}\times\mathbf{n}). \quad (4.4)$$

Since the operators (4.4) are expressed thanks to local and inverse of local surface operators, the implementation of $\boldsymbol{\Lambda}^{\mathrm{sq},N_p,\theta_p}_{+,k_+,\mathcal{Z}_+}$ can be realized locally by introducing some auxiliary surface fields (see Section 5.2). This is an important point since only complex-valued sparse matrices appear at the discrete level in the weak coupling procedure when using $-\boldsymbol{\Lambda}^{\mathrm{sq},N_p,\theta_p}_{+,k_+,\mathcal{Z}_+}$ to approximate $-\widetilde{\boldsymbol{\Lambda}_{+,k_+,\mathcal{Z}_+}}$. This results in an additional low memory storage as well as an efficient implementation when applying this approximate linear operator.

Since $\mathbf{T}_-$ is accurately evaluated, we can consider a simple approximation for $\mathbf{T}_+$. In particular, it was shown in [8] that, in the high-frequency regime, the convergence properties are very similar when using Padé-type or low-order approximations of the linear part of $\mathbf{T}_+$. Therefore, we restrict our study to the zeroth-order approximations (4.2) for the linear part of $\mathbf{T}_+$. In addition, choosing $\boldsymbol{\Lambda}^0_{-,k_-,\mathcal{Z}_-}$ appears as natural. However, it was shown in the acoustic case [8] that the number of GMRES iterations can still be high at some frequencies, which is amplified for high contrast situations. For this reason, we also propose to consider the alternative choice $\boldsymbol{\Lambda}^0_{-,k_+,\mathcal{Z}_+}$ which provides an improved convergence rate as validated in Section 7.

5. Formulations for solving the weak coupling and associated subproblems

We now present the weak coupling formulations. For the interior problem (3.4), we use a variational volume formulation which is more adapted to simulate non homogeneous materials when discretized by high-order finite elements. A boundary element method is considered for the exterior problem (3.5). To this end, we first recall some basic results about the integral representation for Maxwell's equations.

5.1. Basics on integral representation

Let us consider a wavenumber $k \in \mathbb{R}_+^*$ and an impedance $\mathcal{Z} \in \mathbb{R}_+^*$. We denote by G_k the three-dimensional Green's function defined by

$$\forall \mathbf{x} \in \mathbb{R}^3 \setminus \{\mathbf{0}\},\quad G_k(\mathbf{x}) = \frac{e^{\iota k\|\mathbf{x}\|}}{4\pi\,\|\mathbf{x}\|}.$$

The electric and magnetic field potential operators are respectively given by $\forall \mathbf{j} \in \mathbf{H}_t^{-\frac{1}{2}}(\mathrm{div}_\Gamma, \Gamma)$, and $\forall \mathbf{x} \in \mathbb{R}^3 \setminus \Gamma$,

$$\boldsymbol{\mathcal{T}}_k\mathbf{j}(\mathbf{x}) = \int_\Gamma G_k(\mathbf{x}-\mathbf{y})\mathbf{j}(\mathbf{y})\,d\mathbf{y} + \frac{1}{k^2}\boldsymbol{\nabla}\int_\Gamma G_k(\mathbf{x}-\mathbf{y})\mathrm{div}_\Gamma\mathbf{j}(\mathbf{y})\,d\mathbf{y}$$

and

$$\boldsymbol{\mathcal{K}}_k\mathbf{j}(\mathbf{x}) = -\mathbf{curl}\int_\Gamma G_k(\mathbf{x}-\mathbf{y})\mathbf{j}(\mathbf{y})\,d\mathbf{y}.$$

Taking the traces of $\boldsymbol{\mathcal{T}}_k\mathbf{j}$ and $\boldsymbol{\mathcal{K}}_k\mathbf{j}$ on Γ and introducing the electric boundary operator: $\forall \mathbf{j} \in \mathbf{H}_t^{-\frac{1}{2}}(\mathrm{div}_\Gamma,\Gamma)$, and $\forall \mathbf{x}\in\Gamma$,

$$\mathbf{T}_k\mathbf{j}(\mathbf{x}) = \int_\Gamma G_k(\mathbf{x}-\mathbf{y})\mathbf{j}(\mathbf{y})\,d\mathbf{y}\times\mathbf{n}(\mathbf{x}) + \frac{1}{k^2}\boldsymbol{\nabla}\int_\Gamma G_k(\mathbf{x}-\mathbf{y})\mathrm{div}_\Gamma\mathbf{j}(\mathbf{y})\,d\mathbf{y}\times\mathbf{n}(\mathbf{x})$$

and the magnetic boundary operator: $\forall \mathbf{j} \in \mathbf{H}_t^{-\frac{1}{2}}(\mathrm{div}_\Gamma,\Gamma)$ and $\forall \mathbf{x}\in\Gamma$,

$$\mathbf{K}_k\mathbf{j}(\mathbf{x}) = \int_\Gamma \boldsymbol{\nabla}_\mathbf{y} G_k(\mathbf{x}-\mathbf{y})\times\mathbf{j}(\mathbf{y})\,d\mathbf{y}\times\mathbf{n}(\mathbf{x}),$$

we obtain the following results.

Proposition 5.1. *We have the trace relations:*

$$\boldsymbol{\gamma}_t^-\boldsymbol{\mathcal{T}}_k = \boldsymbol{T}_k \quad , \quad \boldsymbol{\gamma}_t^+\boldsymbol{\mathcal{T}}_k = \boldsymbol{T}_k \quad , \quad \boldsymbol{\gamma}_t^-\boldsymbol{\mathcal{K}}_k = -\frac{1}{2}\boldsymbol{Id} + \boldsymbol{K}_k \quad , \quad \boldsymbol{\gamma}_t^+\boldsymbol{\mathcal{K}}_{\boldsymbol{k}} = \frac{1}{2}\boldsymbol{Id} + \boldsymbol{K}_k\ .$$

To derive well-posed integral equation formulations, we need to introduce the integral representation for Maxwell's equations [11, 31].

Proposition 5.2. *Introducing the so-called jump relations across* Γ

$$[\boldsymbol{\gamma}_t\boldsymbol{E}] := \boldsymbol{\gamma}_t^-\boldsymbol{E} - \boldsymbol{\gamma}_t^+\boldsymbol{E_{sc}} \ \text{ and } \ [\boldsymbol{\gamma}_t\boldsymbol{H}] := \boldsymbol{\gamma}_t^-\boldsymbol{H} - \boldsymbol{\gamma}_t^+\boldsymbol{H_{sc}},$$

and assuming that Ω_- *is a homogeneous domain, we then have the following integral representation*

$$\left\{\begin{array}{rcl} \boldsymbol{E} &=& \boldsymbol{E_{inc}} + \imath k\mathcal{Z}\boldsymbol{\mathcal{T}}_k[\boldsymbol{\gamma}_t\boldsymbol{H}] - \boldsymbol{\mathcal{K}}_k[\boldsymbol{\gamma}_t\boldsymbol{E}] \\ \boldsymbol{H} &=& \boldsymbol{H_{inc}} - \boldsymbol{\mathcal{K}}_k[\boldsymbol{\gamma}_t\boldsymbol{H}] - \imath k\mathcal{Z}^{-1}\boldsymbol{\mathcal{T}}_k[\boldsymbol{\gamma}_t\boldsymbol{E}] \end{array}\right. \quad \text{in} \quad \Omega_-\cup\Omega_+, \tag{5.1}$$

with

$$\left\{\begin{array}{rcl} \boldsymbol{E_{inc}} &=& \boldsymbol{0} \\ \boldsymbol{H_{inc}} &=& \boldsymbol{0} \end{array}\right. \quad \text{in} \quad \Omega_-.$$

Once the jump relations are known or estimated on Γ, the representation formulae (5.1) can be used to find the solutions in Ω_+ and in a homogeneous interior domain Ω_-.

5.2. Formulations for solving the weak coupling and the exterior/interior subproblems

Several possible combinations of functional spaces can be considered for $\mathbf{g}_\pm$:

$$(\mathbf{g}_-,\mathbf{g}_+) \in \mathbf{H}_t^{-\frac{1}{2}}(\mathrm{div}_\Gamma,\Gamma)\times\mathbf{H}_t^{-\frac{1}{2}}(\mathrm{rot}_\Gamma,\Gamma),\ (\mathbf{g}_-,\mathbf{g}_+) \in \mathbf{H}_t^{-\frac{1}{2}}(\mathrm{rot}_\Gamma,\Gamma)\times\mathbf{H}_t^{-\frac{1}{2}}(\mathrm{rot}_\Gamma,\Gamma)$$

$$\text{and } (\mathbf{g}_-,\mathbf{g}_+) \in \mathbf{H}_t^{-\frac{1}{2}}(\mathrm{rot}_\Gamma,\Gamma)\times\mathbf{H}_t^{-\frac{1}{2}}(\mathrm{div}_\Gamma,\Gamma).$$

From the functional analysis point of view, the best choice is not obvious. During the numerical simulations in Section 7, it however appears that choosing $\mathbf{g}_\pm \in \mathbf{H}_t^{-\frac{1}{2}}(\mathrm{div}_\Gamma,\Gamma)$ leads to the best convergence properties. Let us mention that alternative approaches such as the Helmholtz decomposition [8] could also be used. The spaces $\mathbf{H}_t^{-\frac{1}{2}}(\mathrm{rot}_\Gamma,\Gamma)$ and $\mathbf{H}_t^{-\frac{1}{2}}(\mathrm{div}_\Gamma,\Gamma)$ are mutually adjoint with respect to the scalar product $\mathbf{L}_t^2(\Gamma)$ [31]. In preparation for the discrete formulation in Section 6, we will however formally identify, in the following proposition, the $\mathbf{H}_t^{-\frac{1}{2}}(\mathrm{div}_\Gamma,\Gamma)$ space with the discrete $\mathbf{H}_t^{-\frac{1}{2}}(\mathrm{div}_\Gamma,\Gamma)$ space which is $\mathbf{L}_t^2(\Gamma)$ with itself.

Proposition 5.3. *Let us consider some test-functions* $\boldsymbol{g}'_- \in \mathbf{H}_t^{-\frac{1}{2}}(\mathrm{div}_\Gamma, \Gamma)$ *and* $\boldsymbol{g}'_+ \in \mathbf{H}_t^{-\frac{1}{2}}(\mathrm{div}_\Gamma, \Gamma)$. *Then, the variational formulation of the weak coupling (3.6) is given by*

$$\left\{ \begin{array}{rcl} \displaystyle\int_\Gamma \boldsymbol{g}_- \cdot \overline{\boldsymbol{g}'_-}\, d\Gamma - \int_\Gamma \boldsymbol{g}_+ \cdot \overline{\boldsymbol{g}'_-}\, d\Gamma - \int_\Gamma (\boldsymbol{T}_- + \boldsymbol{T}_+)\boldsymbol{R}_+ \boldsymbol{g}_+ \cdot \overline{\boldsymbol{g}'_-}\, d\Gamma & = & \boldsymbol{0} \\ \displaystyle\int_\Gamma \boldsymbol{g}_+ \cdot \overline{\boldsymbol{g}'_+}\, d\Gamma - \int_\Gamma \boldsymbol{g}_- \cdot \overline{\boldsymbol{g}'_+}\, d\Gamma + \int_\Gamma (\boldsymbol{T}_- + \boldsymbol{T}_+)\boldsymbol{R}_- \boldsymbol{g}_- \cdot \overline{\boldsymbol{g}'_+}\, d\Gamma & = & \boldsymbol{0} \end{array} \right. . \tag{5.2}$$

The above weak formulation involves the resolution operators $\mathbf{R}_\pm$ associated with the subproblems (3.4) and (3.5). Since the physical parameters of the exterior problem (3.5) are supposed to be constant, the use of surface integral equations is particularly well-adapted. Because the exterior subproblem involves an impedance boundary condition, we consider some specific integral equation formulations. The chosen formulation corresponds to a generalization of the one proposed in [2].

Proposition 5.4. *Let* $\boldsymbol{g} \in \mathbf{H}_t^{-\frac{1}{2}}(\mathrm{div}_\Gamma, \Gamma)$ *and* $(\boldsymbol{E}; \boldsymbol{H}) \in \mathbf{H}_{\mathrm{loc}}(\mathbf{curl}, \overline{\Omega_+})^2$ *such that*

$$\left\{ \begin{array}{rcll} \boldsymbol{curl}\ \boldsymbol{E} - \imath k_+ \mathcal{Z}_+ \boldsymbol{H} & = & \boldsymbol{0} & \text{in } \Omega_+ \\ \boldsymbol{curl}\ \boldsymbol{H} + \imath k_+ \mathcal{Z}_+^{-1} \boldsymbol{E} & = & \boldsymbol{0} & \text{in } \Omega_+ \\ \mathcal{Z}_+ \boldsymbol{H}_{\boldsymbol{sc}} \times \dfrac{\boldsymbol{x}}{||\boldsymbol{x}||} - \boldsymbol{E}_{\boldsymbol{sc}} & = & \underset{r\to+\infty}{\mathcal{O}}(r^{-2}) & \\ \gamma_t^+ \boldsymbol{H} - \boldsymbol{T}_+ \gamma_t^+ \boldsymbol{E} = \boldsymbol{g} & & & \end{array} \right. .$$

We then have:

$$\left\{ \begin{array}{rcl} \frac{1}{2}\boldsymbol{T}_+^{-1}\gamma_t^+ \boldsymbol{H} - \boldsymbol{K}_{k_+}\gamma_t^+ \boldsymbol{E} + \imath k_+ \mathcal{Z}_+ \boldsymbol{T}_{k_+}\gamma_t^+ \boldsymbol{H} & = & \frac{1}{2}\boldsymbol{T}_+^{-1}\boldsymbol{g} + \gamma_t^+ \boldsymbol{E}_{\boldsymbol{inc}} \\ \frac{1}{2}\boldsymbol{T}_+ \gamma_t^+ \boldsymbol{E} - \boldsymbol{K}_{k_+}\gamma_t^+ \boldsymbol{H} - \imath k_+ \mathcal{Z}_+^{-1} \boldsymbol{T}_{k_+}\gamma_t^+ \boldsymbol{E} & = & -\frac{1}{2}\boldsymbol{g} + \gamma_t^+ \boldsymbol{H}_{\boldsymbol{inc}} \end{array} \right. . \tag{5.3}$$

Conversely, if $\boldsymbol{g} \in \mathbf{H}_t^{-\frac{1}{2}}(\mathrm{div}_\Gamma, \Gamma)$, $\boldsymbol{m} \in \mathbf{H}_t^{-\frac{1}{2}}(\mathrm{div}_\Gamma, \Gamma)$, $\boldsymbol{j} \in \mathbf{H}_t^{-\frac{1}{2}}(\mathrm{div}_\Gamma, \Gamma)$ *satisfy*

$$\left\{ \begin{array}{rcl} \frac{1}{2}\boldsymbol{T}_+^{-1}\boldsymbol{j} - \boldsymbol{K}_{k_+}\boldsymbol{m} + \imath k_+ \mathcal{Z}_+ \boldsymbol{T}_{k_+}\boldsymbol{j} & = & \frac{1}{2}\boldsymbol{T}_+^{-1}\boldsymbol{g} + \gamma_t^+ \boldsymbol{E}_{\boldsymbol{inc}} \\ \frac{1}{2}\boldsymbol{T}_+ \boldsymbol{m} - \boldsymbol{K}_{k_+}\boldsymbol{j} - \imath k_+ \mathcal{Z}_+^{-1} \boldsymbol{T}_{k_+}\boldsymbol{m} & = & -\frac{1}{2}\boldsymbol{g} + \gamma_t^+ \boldsymbol{H}_{\boldsymbol{inc}} \end{array} \right. ,$$

then the field $(\boldsymbol{E}; \boldsymbol{H}) \in \mathbf{H}_{\mathrm{loc}}(\mathbf{curl}, \overline{\Omega_+})^2$ *defined by*

$$\left\{ \begin{array}{rcl} \boldsymbol{E} & = & \boldsymbol{E}_{\boldsymbol{inc}} - \imath k_+ \mathcal{Z}_+ \boldsymbol{\mathcal{T}}_{k_+}\boldsymbol{j} + \boldsymbol{\mathcal{K}}_{k_+}\boldsymbol{m} \\ \boldsymbol{H} & = & \boldsymbol{H}_{\boldsymbol{inc}} + \boldsymbol{\mathcal{K}}_{k_+}\boldsymbol{j} + \imath k_+ {\mathcal{Z}_+}^{-1} \boldsymbol{\mathcal{T}}_{k_+}\boldsymbol{m} \end{array} \right. \quad \text{in } \Omega_+$$

is solution of the exterior problem (3.5).

Proof. Let $(\mathbf{E}; \mathbf{H}) \in \mathbf{H}_{\mathrm{loc}}(\mathbf{curl}, \overline{\Omega_+})^2$ be the solution to the exterior problem (3.5). Extending $(\mathbf{E}; \mathbf{H})$ by $(-\mathbf{E}_{\mathbf{inc}}; -\mathbf{H}_{\mathbf{inc}})$ in Ω_-, one gets the following integral representation formulae

$$\left\{ \begin{array}{rcl} \mathbf{E} & = & \mathbf{E}_{\mathbf{inc}} - \imath k_+ \mathcal{Z}_+ \boldsymbol{\mathcal{T}}_{k_+}\gamma_t^+ \mathbf{H} + \boldsymbol{\mathcal{K}}_{k_+}\gamma_t^+ \mathbf{E} \\ \mathbf{H} & = & \mathbf{H}_{\mathbf{inc}} + \boldsymbol{\mathcal{K}}_{k_+}\gamma_t^+ \mathbf{H} + \imath k_+ {\mathcal{Z}_+}^{-1} \boldsymbol{\mathcal{T}}_{k_+}\gamma_t^+ \mathbf{E} \end{array} \right. \quad \text{in } \Omega_+.$$

Taking the tangential traces (5.1) and using the boundary condition, one then obtains (5.3). To prove the equivalence, it is sufficient to remark that the tangential traces of $(\mathbf{E}; \mathbf{H})$ are given by

$$\left\{ \begin{array}{rcl} \gamma_t^+ \mathbf{E} & = & \gamma_t^+ \mathbf{E}_{\mathbf{inc}} - \imath k_+ \mathcal{Z}_+ \mathbf{T}_{k_+}\mathbf{j} + \mathbf{K}_{k_+}\mathbf{m} + \frac{1}{2}\mathbf{m} \\ \gamma_t^+ \mathbf{H} & = & \gamma_t^+ \mathbf{H}_{\mathbf{inc}} + \frac{1}{2}\mathbf{j} + \mathbf{K}_{k_+}\mathbf{j} + \imath k_+ \mathcal{Z}_+^{-1} \mathbf{T}_{k_+}\mathbf{m} \end{array} \right. .$$

A calculation then shows that the boundary condition is fulfilled. ∎

The interior subproblem is solved using a volume variational formulation.

Proposition 5.5. *Denoting by* $\langle\ ;\ \rangle$ *the duality pairing* $\langle \boldsymbol{u};\boldsymbol{v}\rangle = \displaystyle\int_\Gamma \boldsymbol{u}\times\boldsymbol{n}\cdot\boldsymbol{v}\,d\Gamma$ *between* $\mathbf{H}_t^{-\frac{1}{2}}(\mathrm{div}_\Gamma,\Gamma)$ *and itself, the weak volume variational formulation for* $\boldsymbol{E}$ *associated with the interior problem (3.4) is*

$$\begin{aligned}\forall \boldsymbol{v}\in\mathbf{H}(\mathbf{curl},\Omega_-),\ \int_{\Omega_-}\mathbf{curl}\,\boldsymbol{E}\cdot\mathbf{curl}\,\overline{\boldsymbol{v}}\,d\Omega_- - \int_{\Omega_-}k_-^2\,\boldsymbol{E}\cdot\overline{\boldsymbol{v}}\,d\Omega_- \\ -\iota k_-\mathcal{Z}_-\langle\boldsymbol{\gamma}_t^-\overline{\boldsymbol{v}};\boldsymbol{T}_-\boldsymbol{\gamma}_t^-\boldsymbol{E}\rangle = -\iota k_-\mathcal{Z}_-\langle\boldsymbol{\gamma}_t^-\overline{\boldsymbol{v}};\boldsymbol{g}\rangle.\end{aligned} \tag{5.4}$$

The variational formulations of the linear part of the transmission operators based on (4.2) and (4.4) are presented in the following proposition.

Proposition 5.6. *For all test functions* $\boldsymbol{v}\in\mathbf{H}_t^{-\frac{1}{2}}(\mathrm{div}_\Gamma,\Gamma)$*, the weak formulations associated with the linear part of the zeroth-order Taylor transmission conditions and the Padé-localized square-root transmission conditions are respectively defined for* $\boldsymbol{j}\in\mathbf{H}_t^{-\frac{1}{2}}(\mathrm{div}_\Gamma,\Gamma)$ *by*

$$\int_\Gamma \boldsymbol{\Lambda}^0_{\pm,k,\mathcal{Z}}(\boldsymbol{j})\cdot\overline{\boldsymbol{v}}\,d\Gamma = \int_\Gamma \mp\frac{1}{\mathcal{Z}}\boldsymbol{j}\times\boldsymbol{n}\ \cdot\overline{\boldsymbol{v}}\,d\Gamma \tag{5.5}$$

and

$$\int_\Gamma \boldsymbol{\Lambda}^{\mathrm{sq},N_p,\theta_p}_{\pm,k,\mathcal{Z}}(\boldsymbol{j})\cdot\overline{\boldsymbol{v}}\,d\Gamma = \int_\Gamma \mp\frac{1}{\mathcal{Z}}\boldsymbol{r}_k\cdot\overline{\boldsymbol{v}}\,d\Gamma. \tag{5.6}$$

The function $\boldsymbol{r}_k\in\mathbf{H}_t^{-\frac{1}{2}}(\mathrm{curl}_\Gamma,\Gamma)$ *is obtained by solving the following system with auxiliary variables: find* $(\boldsymbol{r}_k,(\boldsymbol{\Psi}_\ell)_{\ell\in\{1;\dots;N_p\}},(\phi_\ell)_{\ell\in\{1;\dots;N_p\}})\in W$ *such that,*
$\forall(\boldsymbol{r}',(\boldsymbol{\Psi}'_\ell)_{\ell\in\{1;\dots;N_p\}},(\phi'_\ell)_{\ell\in\{1;\dots;N_p\}})\in W$*,*

$$\left\{\begin{array}{l}\displaystyle\int_\Gamma C_0\boldsymbol{r}_k\cdot\overline{\boldsymbol{r}'}\,d\Gamma - \int_\Gamma \boldsymbol{j}\times\boldsymbol{n}\cdot\overline{\boldsymbol{r}'}\,d\Gamma + \int_\Gamma\frac{1}{k_\epsilon^2}\mathrm{curl}_\Gamma(\boldsymbol{j}\times\boldsymbol{n})\cdot\mathrm{curl}_\Gamma(\overline{\boldsymbol{r}'})\,d\Gamma \\ \qquad\displaystyle+\sum_{\ell=1}^{N_p}A_\ell\left(\int_\Gamma\boldsymbol{\nabla}_\Gamma\phi_\ell\cdot\overline{\boldsymbol{r}'}\,d\Gamma - \int_\Gamma\frac{1}{k_\epsilon^2}\mathrm{curl}_\Gamma\boldsymbol{\Psi}_\ell\cdot\mathrm{curl}_\Gamma(\overline{\boldsymbol{r}'})\,d\Gamma\right) = \boldsymbol{0} \\ \displaystyle\int_\Gamma\boldsymbol{\Psi}_\ell\cdot\overline{\boldsymbol{\Psi}'_\ell}\,d\Gamma + B_\ell\left(\int_\Gamma\boldsymbol{\nabla}_\Gamma\phi_\ell\cdot\overline{\boldsymbol{\Psi}'_\ell}\,d\Gamma - \int_\Gamma\frac{1}{k_\epsilon^2}\mathrm{curl}_\Gamma\boldsymbol{\Psi}_\ell\cdot\mathrm{curl}_\Gamma(\overline{\boldsymbol{\Psi}'_\ell})\,d\Gamma\right) \\ \qquad\displaystyle-\int_\Gamma\boldsymbol{r}_k\cdot\overline{\boldsymbol{\Psi}'_\ell}\,d\Gamma = \boldsymbol{0}\qquad\forall\ell\in\{1;\dots;N_p\} \\ \displaystyle\int_\Gamma\phi_\ell\cdot\overline{\phi'_\ell}\,d\Gamma + \int_\Gamma\frac{1}{k_\epsilon^2}\boldsymbol{\Psi}_\ell\cdot\boldsymbol{\nabla}_\Gamma\overline{\phi'_\ell}\,d\Gamma = 0\qquad\forall\ell\in\{1;\dots;N_p\}\end{array}\right.,$$

where we set

$$W := \mathbf{H}_t^{-\frac{1}{2}}(\mathrm{curl}_\Gamma,\Gamma)\times[\mathbf{H}_t^{-\frac{1}{2}}(\mathrm{curl}_\Gamma,\Gamma)]^{N_p}\times[\mathrm{H}^1(\Gamma)]^{N_p}.$$

6. Finite element implementation of the weak coupling

Let us now explain the implementation of the electromagnetic weak FEM-BEM coupling. Its discretization is significantly more complex than the acoustic weak FEM-BEM coupling [9] due to the fact that the unknowns $\mathbf{g}_\pm$ are vectorial. More precisely, the main difficulty when discretizing the electromagnetic weak FEM-BEM coupling consists in choosing the representation of $\mathbf{g}_\pm$ at the discrete level.

6.1. Boundary/Finite element discretization

In this paper, the discretization of the surface integral equations is based on a Galerkin boundary element method (BEM). Other approaches can be used as e.g. the collocation and Nyström techniques [11]. Unlike FEM, BEM enjoys a low numerical dispersion because the fundamental solution of the Maxwell's equations is explicitly taken into account in the integral formulations. Therefore, low-order approximation polynomials (typically linear elements) can be used. Conversely, it is well-known that dispersion/pollution errors appear in the numerical solution of FEM when increasing the frequency [30]. As a consequence, the mesh size h strongly depends on the wavenumber k. Using this strategy leads to considering very fine meshes then limiting the use of the standard low-order polynomial basis functions. An alternative way to reduce the error without refining the mesh is to increase the order of the shape functions, where the number of unknowns can still be controlled while keeping an accurate solution. Here, we use such a strategy based on high-order hierarchical finite elements [42]. Among hierarchic shape functions, one of the most popular choices is Lobatto shape functions. They are split into four different types of shape functions: vertex, edge, face and bubble functions. There are several benefits in using the hierarchical shape functions. Indeed, it was shown [42] that they provide good performances while being well-conditioned. Furthermore, their hierarchical nature implies that the shape functions at order $p+1$ are obtained from the shape functions at order p by only adding new shape functions. Thus, one can very simply couple high- and low-order finite elements as well as apply static condensation for bubble shape functions, which vanish on the boundary of each element.

Let us assume that Ω_- is approximated by a computational domain Ω_h using n_t tetrahedral finite elements with n_f faces, n_e edges and n_v vertices. Then, Γ_h, which is the boundary of Ω_h, is composed of n_t^∂ triangles, n_e^∂ edges and n_v^∂ vertices. In order to discretize the weak-coupling, we introduce some finite dimensional approximation subspaces such that $\mathbf{Z}_{h,p} \subset \mathbf{H}_t^{-\frac{1}{2}}(\mathrm{curl}_\Gamma, \Gamma)$, $\mathbf{V}_{h,p} \subset \mathbf{H}_t^{-\frac{1}{2}}(\mathrm{div}_\Gamma, \Gamma)$, $\mathbf{W}_{h,p} \subset \mathbf{H}(\mathbf{curl}, \Omega_-)$ and $Q_h \subset \mathrm{H}^1(\Gamma)$ with

$$\mathbf{Z}_{h,p} := \mathrm{span}\{(\mathbf{z}_j^p)_{1\leq j\leq N_z^p}\}, \text{where } N_z^p = \begin{cases} (p+1)n_e^\partial & p<2 \\ (p+1)n_e^\partial + 3(p-1)n_t^\partial & 2\leq p<3 \\ (p+1)n_e^\partial + (p-1)(p+1)n_t^\partial & 3\leq p \end{cases},$$

$$\mathbf{V}_{h,p} := \mathrm{span}\{(\mathbf{e}_j^p)_{1\leq j\leq N_z^p}\} = \mathrm{span}\{(\mathbf{z}_j^p \times \mathbf{n})_{1\leq j\leq N_z^p}\},$$

$$\mathbf{W}_{h,p} := \mathrm{span}\{(\mathbf{w}_j)_{1\leq j\leq N_w^p}\},$$

$$\text{where } N_w^p = \begin{cases} (p+1)n_e & p<2 \\ (p+1)n_e + 3(p-1)n_f & 2\leq p<3 \\ (p+1)n_e + (p-1)(p+1)n_f + 2(p-1)(p-2)n_t & 3\leq p<4 \\ (p+1)n_e + (p-1)(p+1)n_f + (p-1)(p-2)(p+1)/2n_t & 4\leq p \end{cases}$$

and $Q_h := \mathrm{span}\{(q_j)_{1\leq j\leq n_v^\partial}\}$. The parameter $p \in \mathbb{N}$ designates the polynomial order of the shape functions. Let us remark that $\mathbf{V}_{h,0}$ represents the usual Raviart-Thomas div-conforming space [34]. We define the matrix of the tangential trace operator, denoted by $\mathbb{G}$, as follows

$$\mathbb{G}_{ij} = \begin{cases} 1 & \text{if } \mathbf{w}_{j|\Gamma} = \mathbf{z}_i^p \\ 0 & \text{else} \end{cases}, \quad \text{with } \ 1\leq i\leq N_z^p \ \text{ and } \ 1\leq j\leq N_w^p.$$

We also define by $\{\cdot\}$ the vector of degrees of freedom. We will see in Section 8 that a choice on the polynomial order of the unknowns of the system must be made for stability reasons. To this end,

let us introduce two parameters $(\alpha,\beta)\in\mathbb{N}^2$ *to designate the finite element approximation order.* If $\mathbf{T}_+=\mathbf{\Lambda}^0_{-,k_-,\mathcal{Z}_-}+\mathbf{\Lambda}^{0,\mathbf{inc}}_{-,k_-,\mathcal{Z}_-}$ (the second choice $\mathbf{T}_+=-\mathbf{\Lambda}^0_{+,k_+,\mathcal{Z}_+}-\mathbf{\Lambda}^{0,\mathbf{inc}}_{+,k_+,\mathcal{Z}_+}$ would only slightly change the formulations), then the discretization of the weak formulation (5.2) is defined in the following proposition.

Proposition 6.1. *Let us assume that* $\boldsymbol{T}_+=\mathbf{\Lambda}^0_{-,k_-,\mathcal{Z}_-}+\mathbf{\Lambda}^{0,\mathbf{inc}}_{-,k_-,\mathcal{Z}_-}$. *Then, the discretization of the weak formulation (5.2) is given as follows: find* $(\boldsymbol{g}_{+,h},\boldsymbol{g}_{-,h})\in\boldsymbol{V}_{h,0}\times\boldsymbol{V}_{h,\beta}$ *such that for any test-functions* $(\boldsymbol{e}^0_i)_{i\in\{1,\dots,N^0_z\}}\in\boldsymbol{V}_{h,0}$ *and* $(\boldsymbol{e}^\beta_j)_{j\in\{1,\dots,N^\beta_z\}}\in\boldsymbol{V}_{h,\beta}$,

$$\left\{\begin{array}{ll}\displaystyle\int_{\Gamma_h}\boldsymbol{g}_{-,h}\cdot\boldsymbol{e}^\beta_j d\Gamma_h-\int_{\Gamma_h}\boldsymbol{g}_{+,h}\cdot\boldsymbol{e}^\beta_j d\Gamma_h-\int_{\Gamma_h}(\frac{\boldsymbol{a}_h}{\mathcal{Z}_+}+\frac{\boldsymbol{m}_{+,h}\times\boldsymbol{n}}{\mathcal{Z}_-})\cdot\boldsymbol{e}^\beta_j d\Gamma_h & =\boldsymbol{0}\\ \displaystyle\int_{\Gamma_h}\boldsymbol{g}_{+,h}\cdot\boldsymbol{e}^0_i d\Gamma_h-\int_{\Gamma_h}\boldsymbol{g}_{-,h}\cdot\boldsymbol{e}^0_i d\Gamma_h+\int_{\Gamma_h}(\frac{\boldsymbol{c}_h}{\mathcal{Z}_+}+\frac{\boldsymbol{m}_{-,h}\times\boldsymbol{n}}{\mathcal{Z}_-})\cdot\boldsymbol{e}^0_i d\Gamma_h & =\boldsymbol{0}\end{array}\right.,\tag{6.1}$$

where $\boldsymbol{m}_{+,h}$ *is the total exterior magnetic current solution of formulation (6.2) and*

$$\boldsymbol{m}_{-,h}=\sum_{\ell=1}^{N^\alpha_z}(\mathbb{G}\{\boldsymbol{E}_{-,h}\})_\ell\boldsymbol{z}^\alpha_\ell\times\boldsymbol{n},$$

with $\boldsymbol{E}_{-,h}$ *solution of the weak formulation (6.3).*

If $\boldsymbol{T}_-=-\mathbf{\Lambda}^{\mathrm{sq},N_p,\theta_p}_{+,k_+,\mathcal{Z}_+}-\mathbf{\Lambda}^{\mathrm{sq},\mathbf{inc}}_{+,k_+,\mathcal{Z}_+}$, *then* $\boldsymbol{a}_h$ *and* $\boldsymbol{c}_h$ *are defined through the formulations:*

- *Find* $(\boldsymbol{a}_h,(\mathbf{\Psi}_{\ell,h})_{\ell\in\{1;\dots;N_p\}},(\phi_{\ell,h})_{\ell\in\{1;\dots;N_p\}})\in\boldsymbol{Z}_{h,\beta}\times[\boldsymbol{Z}_{h,\beta}]^{N_p}\times[Q_h]^{N_p}$ *for any test-functions* $(\boldsymbol{z}^\beta_i)_{i\in\{1,\dots,N^\beta_z\}}\in\boldsymbol{Z}_{h,\beta}$ *and* $(q_m)_{m\in\{1,\dots,n^\partial_v\}}\in Q_h$,

$$\left\{\begin{array}{l}\displaystyle\int_{\Gamma_h}C_0\,\boldsymbol{a}_h\cdot\boldsymbol{z}^\beta_i d\Gamma_h-\int_{\Gamma_h}\boldsymbol{m}_{+,h}\times\boldsymbol{n}\cdot\boldsymbol{z}^\beta_i d\Gamma_h+\int_{\Gamma_h}\frac{1}{k^2_\epsilon}\mathrm{curl}_{\Gamma_h}(\boldsymbol{m}_{+,h}\times\boldsymbol{n})\cdot\mathrm{curl}_{\Gamma_h}(\boldsymbol{z}^\beta_i)\\ d\Gamma_h+\displaystyle\sum_{\ell=1}^{N_p}A_\ell\left(\int_{\Gamma_h}\boldsymbol{\nabla}_{\Gamma_h}\phi_{\ell,h}\cdot\boldsymbol{z}^\beta_i d\Gamma_h-\int_{\Gamma_h}\frac{1}{k^2_\epsilon}\mathrm{curl}_{\Gamma_h}\mathbf{\Psi}_{\ell,h}\cdot\mathrm{curl}_{\Gamma_h}(\boldsymbol{z}^\beta_i)d\Gamma_h\right)=\boldsymbol{0}\\ \displaystyle\int_{\Gamma_h}\mathbf{\Psi}_{\ell,h}\cdot\boldsymbol{z}^\beta_i d\Gamma_h+B_\ell\left(\int_{\Gamma_h}\boldsymbol{\nabla}_{\Gamma_h}\phi_\ell\cdot\boldsymbol{z}^\beta_i d\Gamma_h-\int_{\Gamma_h}\frac{1}{k^2_\epsilon}\mathrm{curl}_{\Gamma_h}\mathbf{\Psi}_{\ell,h}\cdot\mathrm{curl}_{\Gamma_h}(\boldsymbol{z}^\beta_i)d\Gamma_h\right)\cdot\\ \qquad\qquad\displaystyle-\int_{\Gamma_h}\boldsymbol{a}_h\cdot\boldsymbol{z}^\beta_i d\Gamma_h=\boldsymbol{0}\qquad\forall\ell\in\{1;\dots;N_p\}\\ \\ \displaystyle\int_{\Gamma_h}\phi_\ell\cdot q_m d\Gamma_h+\int_{\Gamma_h}\frac{1}{k^2_\epsilon}\mathbf{\Psi}_\ell\cdot\boldsymbol{\nabla}_{\Gamma_h}q_m d\Gamma_h=0\qquad\forall\ell\in\{1;\dots;N_p\}\end{array}\right.$$

- *Find* $(\boldsymbol{c}_h,(\boldsymbol{\chi}_{\ell,h})_{\ell\in\{1;\dots;N_p\}},(\psi_{\ell,h})_{\ell\in\{1;\dots;N_p\}})\in\boldsymbol{Z}_{h,\beta}\times[\boldsymbol{Z}_{h,\beta}]^{N_p}\times[Q_h]^{N_p}$ *for any test-functions* $(\boldsymbol{z}^\beta_i)_{i\in\{1,\dots,N^\beta_z\}}\in\boldsymbol{Z}_{h,\beta}$ *and* $(q_m)_{m\in\{1,\dots,n^\partial_v\}}\in Q_h$,

$$
\left\{
\begin{array}{l}
\displaystyle\int_{\Gamma_h} C_0\, \boldsymbol{c}_h \cdot \boldsymbol{z}_i^\beta d\Gamma_h - \int_{\Gamma_h} \boldsymbol{m}_{-,h} \times \boldsymbol{n} \cdot \boldsymbol{z}_i^\beta d\Gamma_h + \int_{\Gamma_h} \frac{1}{k_\epsilon^2} \mathrm{curl}_{\Gamma_h}(\boldsymbol{m}_{-,h} \times \boldsymbol{n}) \cdot \mathrm{curl}_{\Gamma_h}(\boldsymbol{z}_i^\beta) \\
d\Gamma_h + \displaystyle\sum_{\ell=1}^{N_p} A_\ell \left(\int_{\Gamma_h} \boldsymbol{\nabla}_{\Gamma_h} \psi_{\ell,h} \cdot \boldsymbol{z}_i^\beta d\Gamma_h - \int_{\Gamma_h} \frac{1}{k_\epsilon^2} \mathrm{curl}_{\Gamma_h} \boldsymbol{\chi}_{\ell,h} \cdot \mathrm{curl}_{\Gamma_h}(\boldsymbol{z}_i^\beta) d\Gamma_h \right) = \boldsymbol{0} \\
\displaystyle\int_{\Gamma_h} \boldsymbol{\chi}_{\ell,h} \cdot \boldsymbol{z}_i^\beta d\Gamma_h + B_\ell \left(\int_{\Gamma_h} \boldsymbol{\nabla}_{\Gamma_h} \psi_\ell \cdot \boldsymbol{z}_i^\beta d\Gamma_h - \int_{\Gamma_h} \frac{1}{k_\epsilon^2} \mathrm{curl}_{\Gamma_h} \boldsymbol{\chi}_{\ell,h} \cdot \mathrm{curl}_{\Gamma_h}(\boldsymbol{z}_i^\beta) d\Gamma_h \right) \cdot \\
\qquad\qquad - \displaystyle\int_{\Gamma_h} \boldsymbol{c}_h \cdot \boldsymbol{z}_i^\beta d\Gamma_h = \boldsymbol{0} \qquad \forall \ell \in \{1; ...; N_p\} \\
\displaystyle\int_{\Gamma_h} \psi_\ell \cdot q_m d\Gamma_h + \int_{\Gamma_h} \frac{1}{k_\epsilon^2} \boldsymbol{\chi}_\ell \cdot \boldsymbol{\nabla}_{\Gamma_h} q_m d\Gamma_h = 0 \qquad \forall \ell \in \{1; ...; N_p\}
\end{array}
\right.
$$

If $\boldsymbol{T}_- = -\boldsymbol{\Lambda}^0_{+,k_+,\mathcal{Z}_+} - \boldsymbol{\Lambda}^{0,\mathbf{inc}}_{+,k_+,\mathcal{Z}_+}$, *then we more simply have:* $\boldsymbol{a}_h = \boldsymbol{m}_{+,h} \times \boldsymbol{n}$ *and* $\boldsymbol{c}_h = \boldsymbol{m}_{-,h} \times \boldsymbol{n}$.

The discrete weak formulation of the integral equations (5.3) is defined in the following proposition.

Proposition 6.2. *Find* $(\boldsymbol{m}_{+,h}, \boldsymbol{j}_{+,h}) \in \boldsymbol{V}_{h,0} \times \boldsymbol{V}_{h,0}$ *such that for any test-function* $(\boldsymbol{e}_i^0)_{i \in \{1,...,N_z^0\}} \in \boldsymbol{V}_{h,0}$,

$$
\left\{
\begin{array}{l}
\displaystyle\frac{1}{2} \int_{\Gamma_h} \boldsymbol{j}_{+,h} \cdot \boldsymbol{e}_i^0 d\Gamma_h - \int_{\Gamma_h} (\boldsymbol{K}_{k_+} \frac{\boldsymbol{m}_{+,h}}{\mathcal{Z}_-}) \times \boldsymbol{n} \cdot \boldsymbol{e}_i^0 d\Gamma_h + \iota \int_{\Gamma_h} k_+ \frac{\mathcal{Z}_+}{\mathcal{Z}_-} (\mathbf{T}_{k_+} \boldsymbol{j}_{+,h}) \times \boldsymbol{n} \\
\qquad\qquad \cdot \boldsymbol{e}_i^0 d\Gamma_h = \displaystyle\frac{1}{2} \int_{\Gamma_h} \boldsymbol{g}_{+,h} \cdot \boldsymbol{e}_i^0 d\Gamma_h + \int_{\Gamma_h} \mathcal{Z}_-^{-1} \boldsymbol{\gamma}_t^+ \boldsymbol{E}_{\boldsymbol{inc}} \times \boldsymbol{n} \cdot \boldsymbol{e}_i^0 d\Gamma_h \\
\displaystyle\frac{1}{2} \int_{\Gamma_h} \frac{\boldsymbol{m}_{+,h}}{\mathcal{Z}_-} \cdot \boldsymbol{e}_i^0 d\Gamma_h + \int_{\Gamma_h} (\boldsymbol{K}_{k_+} \boldsymbol{j}_{+,h}) \times \boldsymbol{n} \cdot \boldsymbol{e}_i^0 d\Gamma_h + \iota \int_{\Gamma_h} k_+ \frac{\mathcal{Z}_-}{\mathcal{Z}_+} (\mathbf{T}_{k_+} \frac{\boldsymbol{m}_{+,h}}{\mathcal{Z}_-}) \times \boldsymbol{n} \\
\qquad\qquad \cdot \boldsymbol{e}_i^0 d\Gamma_h = \displaystyle\frac{1}{2} \int_{\Gamma_h} \boldsymbol{g}_{+,h} \times \boldsymbol{n} \cdot \boldsymbol{e}_i^0 d\Gamma_h - \int_{\Gamma_h} \boldsymbol{\gamma}_t^+ \boldsymbol{H}_{\boldsymbol{inc}} \times \boldsymbol{n} \cdot \boldsymbol{e}_i^0 d\Gamma_h
\end{array}
\right. . \tag{6.2}
$$

Finally, we discretize the variational formulation (5.4) as follows.

Proposition 6.3. *Find* $\boldsymbol{E}_{-,h} \in \boldsymbol{W}_{h,\alpha}$ *such that for any test-function* $(\boldsymbol{w}_i)_{i \in \{1,...,N_w\}} \in \boldsymbol{W}_{h,\alpha}$,

$$
\begin{aligned}
\int_{\Omega_h} \mathbf{curl}\, \boldsymbol{E}_{-,h} \cdot \mathbf{curl}\, \boldsymbol{w}_i d\Omega_h - \int_{\Omega_h} k_-^2 \boldsymbol{E}_{-,h} \cdot \boldsymbol{w}_i d\Omega_h + \iota \int_{\Gamma_h} k_- \frac{\mathcal{Z}_-}{\mathcal{Z}_+} \boldsymbol{c}_h \cdot \mathbb{G} \boldsymbol{w}_i d\Gamma_h = \\
\iota \int_{\Gamma_h} k_- \mathcal{Z}_- \boldsymbol{g}_{-,h} \cdot \mathbb{G} \boldsymbol{w}_i d\Gamma_h
\end{aligned} \tag{6.3}
$$

.

6.2. The weak coupling algorithm

In order to have a more compact expression in the discrete setting of the Jacobi algorithm (3.7)-(3.9) at iteration $n+1$, we introduce the two families of operators $\mathscr{R}_\pm$, $\mathscr{S}_\pm$ such that:

$$
\begin{array}{l}
\{\mathbf{E}_+^{n+1}\} = \mathscr{R}_+(\{\mathbf{E_{inc}}\}, \{\mathbf{g}_+^n\}), \\
\{\mathbf{E}_-^{n+1}\} = \mathscr{R}_-(\{\mathbf{0}\}, \{\mathbf{g}_-^n\}), \\
\begin{pmatrix} \{\mathbf{g}_-^{n+1}\} \\ \{\mathbf{g}_+^{n+1}\} \end{pmatrix} = \begin{pmatrix} \mathscr{S}_-(\{\mathbf{g}_+^n\}, \{\mathbf{E}_+^{n+1}\}) \\ \mathscr{S}_+(\{\mathbf{g}_-^n\}, \{\mathbf{E}_-^{n+1}\}) \end{pmatrix},
\end{array}
$$

where $\{\mathbf{E}_-^{n+1}\}$, $\{(\mathbf{E}_+^{n+1}\}$ and $\begin{pmatrix}\{\mathbf{g}_-^{n+1}\}\\ \{\mathbf{g}_+^{n+1}\}\end{pmatrix}$ are the solutions of the finite element discretizations (6.3), (6.2) and (6.1), respectively. By linearity of the equations, we decompose the field $\{\mathbf{E}_\pm^{n+1}\}$ as

$$\{\mathbf{E}_\pm^{n+1}\} = \{\widetilde{\mathbf{E}}_\pm^{n+1}\} + \{\mathring{\mathbf{E}}_\pm^{n+1}\},$$

where

$$\{\widetilde{\mathbf{E}}_-^{n+1}\} = \mathscr{R}_-(\{\mathbf{0}\},\{\mathbf{0}\}), \quad \{\widetilde{\mathbf{E}}_+^{n+1}\} = \mathscr{R}_+(\{\mathbf{E_{inc}}\},\{\mathbf{0}\}), \quad \{\mathring{\mathbf{E}}_\pm^{n+1}\} = \mathscr{R}_\pm(\{\mathbf{0}\},\{\mathbf{g}_\pm^n\}).$$

The quantities $\{\widetilde{\mathbf{E}}_\pm^{n+1}\}$ are independent of the iteration number n and can hence be written as $\{\widetilde{\mathbf{E}}_\pm\} := \{\widetilde{\mathbf{E}}_\pm^{n+1}\}$, $\forall n \in \mathbb{N}$. Therefore, $\{\mathbf{g}_\pm^{n+1}\}$ is such that

$$\{\mathbf{g}_\pm^{n+1}\} = \mathscr{S}_\pm(\{\mathbf{g}_\mp^n\},\{\mathring{\mathbf{E}}_\mp^{n+1}\}) + \mathscr{S}_\pm(\{\mathbf{0}\},\{\widetilde{\mathbf{E}}_\mp\}).$$

One iteration of the weak coupling algorithm then corresponds to

$$\begin{pmatrix}\{\mathbf{g}_-^{n+1}\}\\ \{\mathbf{g}_+^{n+1}\}\end{pmatrix} = \boldsymbol{\mathcal{A}}\begin{pmatrix}\{\mathbf{g}_-^{n}\}\\ \{\mathbf{g}_+^{n}\}\end{pmatrix} + \begin{pmatrix}\mathbf{b}_-\\ \mathbf{b}_+\end{pmatrix},$$

where the quantities $\boldsymbol{\mathcal{A}}\begin{pmatrix}\{\mathbf{g}_-^{n}\}\\ \{\mathbf{g}_+^{n}\}\end{pmatrix}$ are given by

$$\boldsymbol{\mathcal{A}}\begin{pmatrix}\{\mathbf{g}_-^{n}\}\\ \{\mathbf{g}_+^{n}\}\end{pmatrix} = \begin{pmatrix}\mathscr{S}_-(\{\mathbf{g}_+^n\},\{\mathring{\mathbf{E}}_+^{n+1}\})\\ \mathscr{S}_+(\{\mathbf{g}_-^n\},\{\mathring{\mathbf{E}}_-^{n+1}\})\end{pmatrix}.$$

The information about the incident plane wave is contained in the right-hand side:

$$\begin{pmatrix}\mathbf{b}_-\\ \mathbf{b}_+\end{pmatrix} = \begin{pmatrix}\mathscr{S}_-(\{\mathbf{0}\},\{\widetilde{\mathbf{E}}_+\})\\ \mathscr{S}_+(\{\mathbf{0}\},\{\widetilde{\mathbf{E}}_-\}.\end{pmatrix}.$$

The whole weak coupling algorithm can then be recast into a linear system:

$$(\mathbf{Id} - \boldsymbol{\mathcal{A}})\begin{pmatrix}\{\mathbf{g}_-\}\\ \{\mathbf{g}_+\}\end{pmatrix} = \begin{pmatrix}\mathbf{b}_-\\ \mathbf{b}_+\end{pmatrix}$$

which can be solved for example by a GMRES iterative solver. Algorithm 1 summarizes the above procedure.

7. Numerical results

We present in this section some numerical examples to validate and analyze the behaviour of the weak FEM-BEM coupling algorithm 1. All the numerical tests were performed using `GmshFEM` [36], a newly developed open-source finite element library based on `Gmsh` [19] and the open-source boundary element library `Bempp-cl` [39]. Three scatterers are considered: the unit sphere, the unit cube and the same cube with a reentrant corner (see Fig. 2). The objects are illuminated by an electromagnetic plane wave defined by

$$\mathbf{E}_{\mathbf{inc}}(\mathbf{x}) = \mathbf{p}e^{\imath k_+ \boldsymbol{\sigma}_{\mathbf{inc}}\cdot\mathbf{x}},$$

Algorithm 1: Weak coupling algorithm with Krylov solver.

1. Compute the right-hand side $\begin{pmatrix}\mathbf{b}_-\\ \mathbf{b}_+\end{pmatrix}$.

2. Solve the linear system

$$(\mathbf{Id} - \boldsymbol{\mathcal{A}}) \begin{pmatrix}\{\mathbf{g}_-\}\\ \{\mathbf{g}_+\}\end{pmatrix} = \begin{pmatrix}\mathbf{b}_-\\ \mathbf{b}_+\end{pmatrix}$$

by using a Krylov subspace iterative solver (GMRES) [37]. At each iteration, solve the subproblems associated with the systems (6.3) and (6.2).

3. At convergence, compute the solution

$$\{\mathbf{E}_\pm\} = \mathscr{R}_\pm(\{\mathbf{E_{inc}}\}), \{\mathbf{0}\}) + \mathscr{R}_\pm(\{\mathbf{0}\}), \{\mathbf{g}_\pm\}) = \mathscr{R}_\pm(\{\mathbf{E_{inc}}\}), \{\mathbf{g}_\pm\}).$$

where $\mathbf{p} = (1,0,0)^T$ is the polarization vector and $\boldsymbol{\sigma}_{\mathbf{inc}} = (0,0,1)^T$ is the incidence vector. In the following, we also evaluate the far-field solution through the bistatic Radar Cross Section (RCS) defined by

$$\mathrm{RCS}(\boldsymbol{\sigma}, \boldsymbol{\sigma}_{\mathbf{inc}}) := 10\log_{10}(4\pi \lim_{r\to+\infty} r^2 \frac{\|\mathbf{E_{sc}}(r,\theta,\phi)\|^2}{\|\mathbf{E_{inc}}\|^2}) \quad (\mathrm{dB}),$$

where $\boldsymbol{\sigma}(\theta,\phi) = (\sin(\theta)\cos(\phi), \sin(\theta)\sin(\phi), \cos(\theta))^T$ and (r,θ,ϕ) are the spherical coordinates. For all the presented examples, the GMRES (without restart) iterations are stopped when the initial residual has decreased by a factor of 10^{-4} to get an accurate RCS, and we fix the maximum number of iterations to 200. We designate by $(\widetilde{\mathbf{T}_-}; \widetilde{\mathbf{T}_+})_\alpha^\beta$ the linear part of the transmission operators selected when considering the finite element approximation order $(\alpha;\beta)$ as described in Section 6. We define the mesh size $h = \lambda/n_\lambda$, with $\lambda := \min(\lambda_-;\lambda_+)$, setting $\lambda_\pm = 2\pi/k_\pm$ and where n_λ is the number of points per wavelength λ. We always assume that the exterior domain is made up of air so that $\mathcal{Z}_+ = \mathcal{Z}_0$.

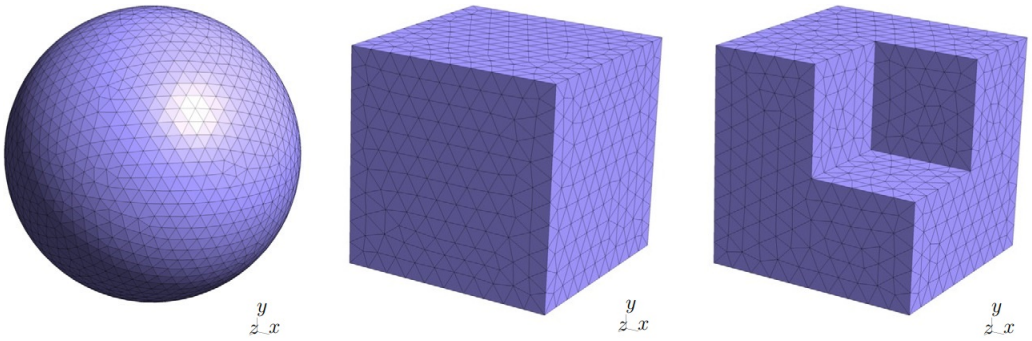

Figure 2: Scatterer geometries: sphere, cube and cube with reentrant corner.

7.1. Homogeneous scatterers

Let us start by considering the unit sphere for the parameters: $\mathcal{Z}_- = \frac{1}{2}\mathcal{Z}_+$, $k_- = 2k_+$ and $n_\lambda = 5$. We report in Fig. 3 the number of GMRES iterations for the weak FEM-BEM coupling

vs the exterior wavenumber k_+ for the operators $(-\mathbf{\Lambda}^{\mathrm{sq},N_p,\theta_p}_{+,k_+,\mathcal{Z}_+};\mathbf{\Lambda}^{0}_{-,k_-,\mathcal{Z}_-})^3_2$ (some comparisons with the choice $\widetilde{\mathbf{T}_+} = -\mathbf{\Lambda}^0_{+,k_+,\mathcal{Z}_+}$ will be analyzed later). Several pairs of Padé parameters $(N_p;\theta_p)$ are considered. We observe that $\theta_p = \frac{\pi}{2}$ leads to the best convergence and $N_p = 2$ terms are sufficient for the Padé expansion. In the following examples, we will always consider $\theta_p = \frac{\pi}{2}$ and $N_p = 4$.

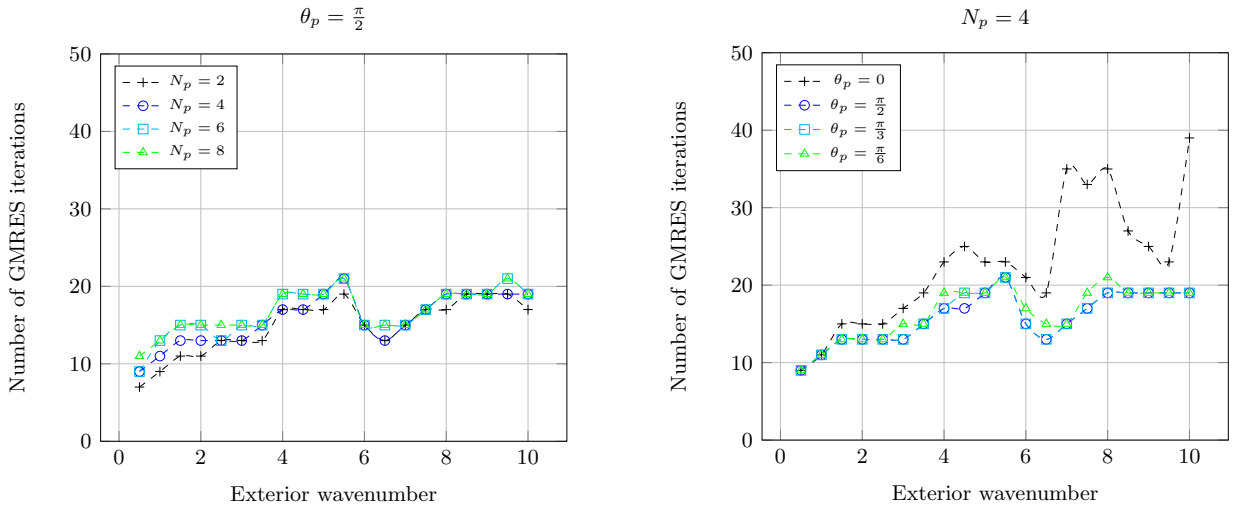

Figure 3: Influence of parameters N_p and θ_p on the convergence of the weak FEM-BEM coupling.

Now, we fix the parameters $\mathcal{Z}_- = \frac{1}{2}\mathcal{Z}_+$, $k_- = 2$ and $k_+ = 1$, for the unit cube. Fig. 4 shows the influence of the FEM approximation orders $(\alpha;\beta)$ on the convergence of the weak FEM-BEM coupling with $(-\mathbf{\Lambda}^{\mathrm{sq},N_p,\theta_p}_{+,k_+,\mathcal{Z}_+};\mathbf{\Lambda}^{0}_{-,k_-,\mathcal{Z}_-})^\beta_\alpha$. The first graph presents the evolution of the number of GMRES iterations in terms of discretization density n_λ, where $\alpha = 2$ and $\beta := 0, ..., 3$. We see that for $\beta = 0$ and $\beta = 1$ the number of iterations strongly increases with n_λ. For $\beta = 2$ and $\beta = 3$ on the other hand, we observe a convergence rate that is independent of n_λ, which is an important property for practical problems when refining the mesh. Since the GMRES convergence strongly depends on the spectral properties of the linear part of the weak coupling operator $(\mathbf{Id} - \boldsymbol{\mathcal{S}}_\pi)$, the choice of the discretization parameters $(\alpha;\beta)$ impacts the eigenvalue distribution. To illustrate this point, we report in the second graph the eigenvalues distribution of the linear part of $(\mathbf{Id} - \boldsymbol{\mathcal{S}}_\pi)$ in the complex plane when $n_\lambda = 10$. For the pair $(\alpha = 2;\beta = 0)$, the convergence is achieved in 62 iterations, which can be explained by the fact that there are eigenvalues with a negative real part. On the other hand, the pair $(\alpha = 2;\beta = 3)$ leads to an excellent convergence in 9 iterations with a large number of eigenvalues clustering around $(1, 0)$. Since $\mathbf{\Lambda}^0_{-,k_-,\mathcal{Z}_-}$ is a rough approximation of $\widetilde{\mathbf{\Lambda}_{-,k_-,\mathcal{Z}_-}}$, there are also a few eigenvalues distant from $(1, 0)$ but the linear part of $(\mathbf{Id} - \boldsymbol{\mathcal{S}}_\pi)$ remains quasi-nilpotent since $\mathbf{\Lambda}^{\mathrm{sq},N_p,\theta_p}_{+,k_+,\mathcal{Z}_+}$ is an accurate approximation of $\widetilde{\mathbf{\Lambda}_{+,k_+,\mathcal{Z}_+}}$. The numerical results from Fig. 4 suggest that β must fulfill: $\beta \geq \alpha$.

Our goal is now to compare the different transmission operators involved in the formulations, most particularly according to the contrast parameter $\delta = k_-/k_+$. From now on, we always indicate on the figures the values of the physical parameters $k_\pm$ and $\mathcal{Z}_\pm$, and the mesh size n_λ. In addition, to simplify the presentation, we introduce the shorter notations: $\mathbf{\Lambda}^0_\pm := \mathbf{\Lambda}^0_{\pm,k_\pm,\mathcal{Z}_\pm}$, and $\mathbf{\Lambda}^{\mathrm{sq}}_+ := \mathbf{\Lambda}^{\mathrm{sq},N_p,\theta_p}_{+,k_+,\mathcal{Z}_+}$, with $N_p = 4$ and $\theta_p = \pi/2$. We present in Fig. 5 the behavior of the weak FEM-BEM coupling for different values of δ. In the case of high-contrast scattering problems, we can clearly see that, as mentioned in Section 3, using $\widetilde{\mathbf{T}_+} = -\mathbf{\Lambda}^0_+$ is more efficient than $\widetilde{\mathbf{T}_+} = \mathbf{\Lambda}^0_-$.

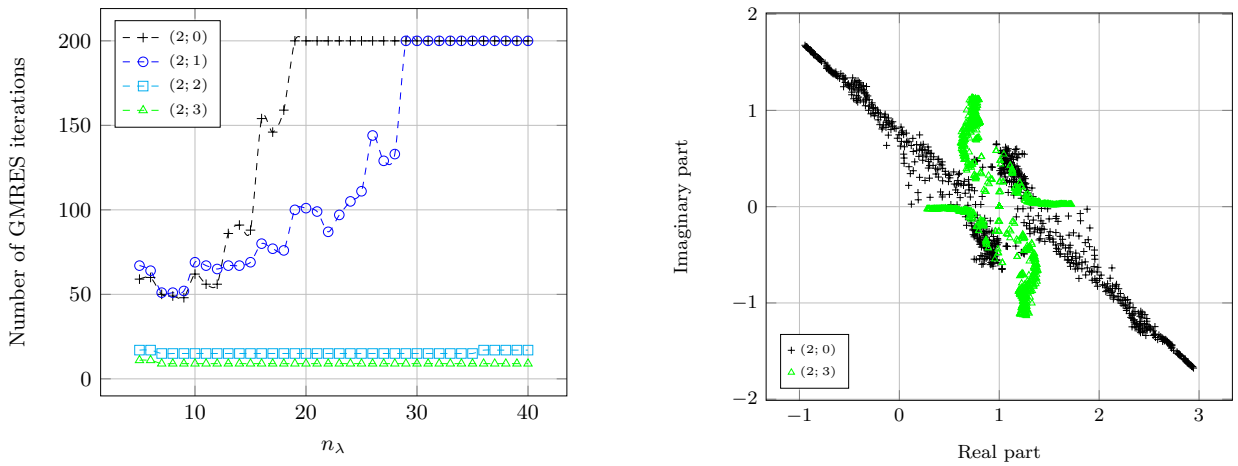

Figure 4: Influence of parameters (α;β) on the convergence of the weak FEM-BEM coupling.

This is even more pronounced when increasing β. To illustrate this property, we set $\widetilde{\mathbf{T}_-} = -\mathbf{\Lambda}_+^{\mathrm{sq}}$, with $\alpha = 2$ and $\beta = 4$. We consider an impedance parameter $\mathcal{Z}_x$ which varies between 10 and 5×10^4. We report in Fig. 6 the evolution of the number of GMRES iterations for the operators $\widetilde{\mathbf{T}_+} = \mathcal{Z}_x^{-1}(\mathbf{Id} \times \mathbf{n})$ corresponding to various values $\mathcal{Z}_x$, for a contrast $\delta = 13$. We observe that the number of iterations is minimal in an interval where $\mathcal{Z}_+$ seems to be a good approximation of the left point of this interval. Conversely, the value $\mathcal{Z}_-$ is not a suitable choice since it is out of this range of optimal values. Fig. 7 shows the evolution of the number of GMRES iterations with respect to the exterior wavenumber k_+. We observe that $(-\mathbf{\Lambda}_+^{\mathrm{sq}}; -\mathbf{\Lambda}_+^0)_2^3$ leads to the lowest dependency of the GMRES iterations with respect to the exterior wavenumber. Let us remark that the convergence rates for both $(-\mathbf{\Lambda}_+^{\mathrm{sq}}; -\mathbf{\Lambda}_+^0)_2^3$ and $(-\mathbf{\Lambda}_+^{\mathrm{sq}}; \mathbf{\Lambda}_-^0)_2^3$ are quasi-identical since the contrast material $\delta = 2$ is low. As it can be seen from Figures 5 and 7, the increase of the number of iterations is more significant for the cube and the cube with reentrant corner than for the sphere. This is due to the fact that the approximations (4.1) are *a priori* formally derived for smooth and convex objects. Fig. 8 shows the evolution of the number of GMRES iterations according to the discretization density n_λ. For $(-\mathbf{\Lambda}_+^{\mathrm{sq}}; \mp\mathbf{\Lambda}_\pm^0)_2^3$, the rate of convergence is mesh independent while it clearly deteriorates with $(-\mathbf{\Lambda}_+^0; \mp\mathbf{\Lambda}_\pm^0)_2^3$. From these results, we conclude that the weak FEM-BEM coupling with the choice of operators $(-\mathbf{\Lambda}_+^{\mathrm{sq}}; -\mathbf{\Lambda}_+^0)_\alpha^\beta$, for $\beta > \alpha$, is very robust and well-suited for solving high-frequency and high-contrast scattering problems.

In order to validate the weak FEM-BEM coupling, the relative errors in $\mathbf{L}_t^2(\Gamma)$-norm between the analytical (*via* a Mie series expansion [5]) and numerical electric/magnetic currents are computed in the sphere case for different densities n_λ (see Fig. 9). We designate by $e_{\boldsymbol{\gamma}_t^- \mathbf{H}}$ and $e_{\boldsymbol{\gamma}_t^- \mathbf{E}}$ the relative errors associated with the electric and magnetic currents, respectively. We remark a lower accuracy of the magnetic current for the cube and the cube with reentrant corner. However, this loss of accuracy can easily be solved by considering the interior problem (2.1a) with known numerical surface electric current during a post-processing step. In Fig. 10, we draw $\mathrm{RCS}(\boldsymbol{\sigma}(\theta, 0), \boldsymbol{\sigma}_{\mathbf{inc}})$ as a function of the angle θ (i.e. in the plane $\{x_2 = 0\}$) for different GMRES tolerances and for the recommended operators $(-\mathbf{\Lambda}_+^{\mathrm{sq}}; -\mathbf{\Lambda}_+^0)_2^3$. For the sphere, the reference analytical far-field [5] is also computed. As expected, the results confirm that the RCS converges when the GMRES tolerance decreases and that a tolerance of 10^{-4} is enough to get an accurate RCS.

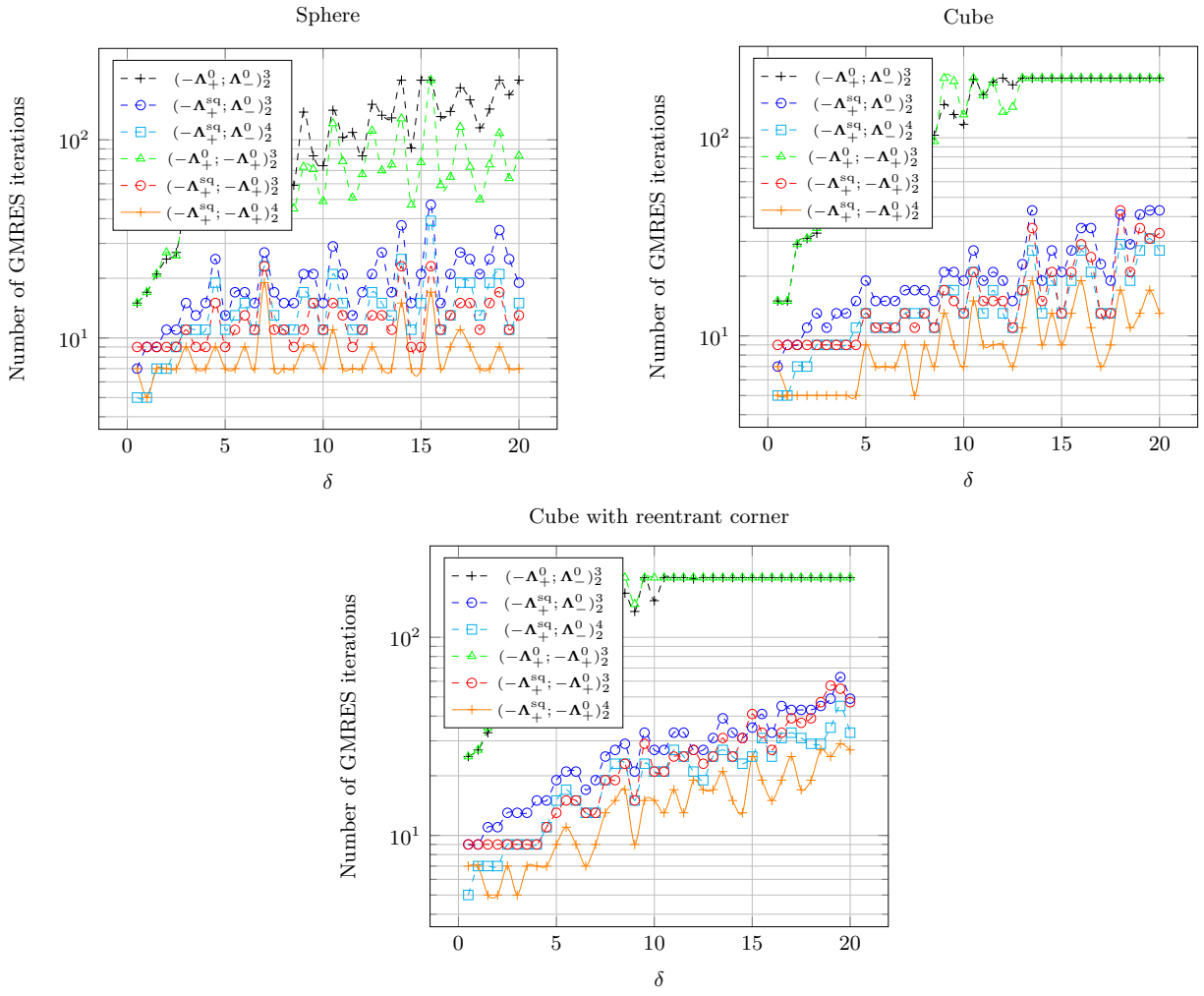

Figure 5: Number of GMRES iterations for the weak FEM-BEM coupling vs the contrast parameter δ (with $k_- = \delta k_+$, $\mathcal{Z}_- = \mathcal{Z}_+/\delta$, $n_\lambda = 5$).

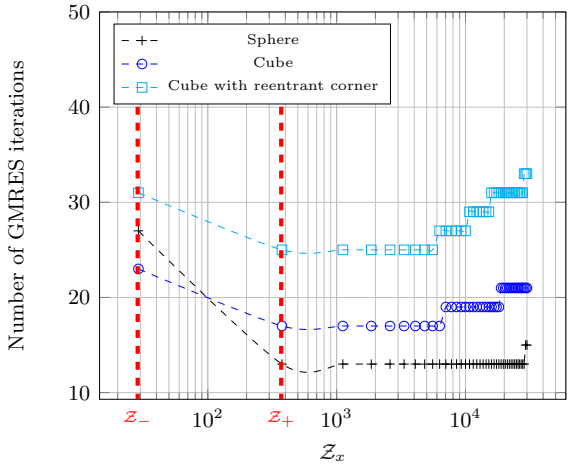

Figure 6: Iteration counts of the weak FEM-BEM coupling for different scatterers as a function of $\mathcal{Z}_x$ (with $k_- = 13$, $k_+ = 1$, $\mathcal{Z}_- = \mathcal{Z}_+/13$, $n_\lambda = 5$).

7.2. Inhomogeneous scatterers

To end, we analyze the case of inhomogeneous scatterers. More specifically, we choose k_- and $\mathcal{Z}_-$ as the space dependent functions given by

$$k_- = \delta k_+ e^{-\|\mathbf{x}\|^2}, \qquad \mathcal{Z}_- = \frac{\mathcal{Z}_+}{\delta} e^{\|\mathbf{x}\|^2},$$

with contrast parameter $\delta \in \mathbb{R}_+^*$. The values of k_+, δ and n_λ are indicated on the figures. We present in Fig. 11 the behavior of the weak FEM-BEM coupling for different contrast parameters δ. In Fig. 12, we report the number of GMRES iterations required for solving the weak FEM-BEM coupling as a function of the exterior wavenumber k_+. Fig. 13 shows the effect of the mesh refinement n_λ over the number of GMRES iterations. Finally, we plot on Fig. 14 the bistatic RCS obtained with various GMRES tolerances for the operators $(-\mathbf{\Lambda}_+^{\mathrm{sq}}; -\mathbf{\Lambda}_+^0)_2^3$. As can be seen on these different figures, we conclude that we obtain results similar to the ones for the homogeneous case.

8. Conclusion

In this work, we proposed a new well-conditioned weak coupling of boundary element and high-order finite element methods for time-harmonic electromagnetic scattering. The weak coupling was formulated as a non-overlapping Schwarz domain decomposition method, where the transmission conditions are constructed through Padé localized approximations of the Magnetic-to-Electric operators. Numerical results validating the new approach are presented for both homogeneous and inhomogeneous obstacles. The number of iterations required to solve the weak FEM-BEM coupling is only slightly dependent on the frequency, the mesh size and the contrast coefficient. Extensions to scatterers with partially coated boundaries and coupling with H-matrix solvers are currently underway.

Acknowledgments. This work was supported by Thales Defence Mission Systems (DMS) through the CIFRE contracts 2015/0197 and 2018/1609. This work was funded in part through an ARC grant for Concerted Research Actions (ARC WAVES 15/19-03), financed by the Wallonia-Brussels Federation of Belgium. Computational resources have been provided by the Consortium des

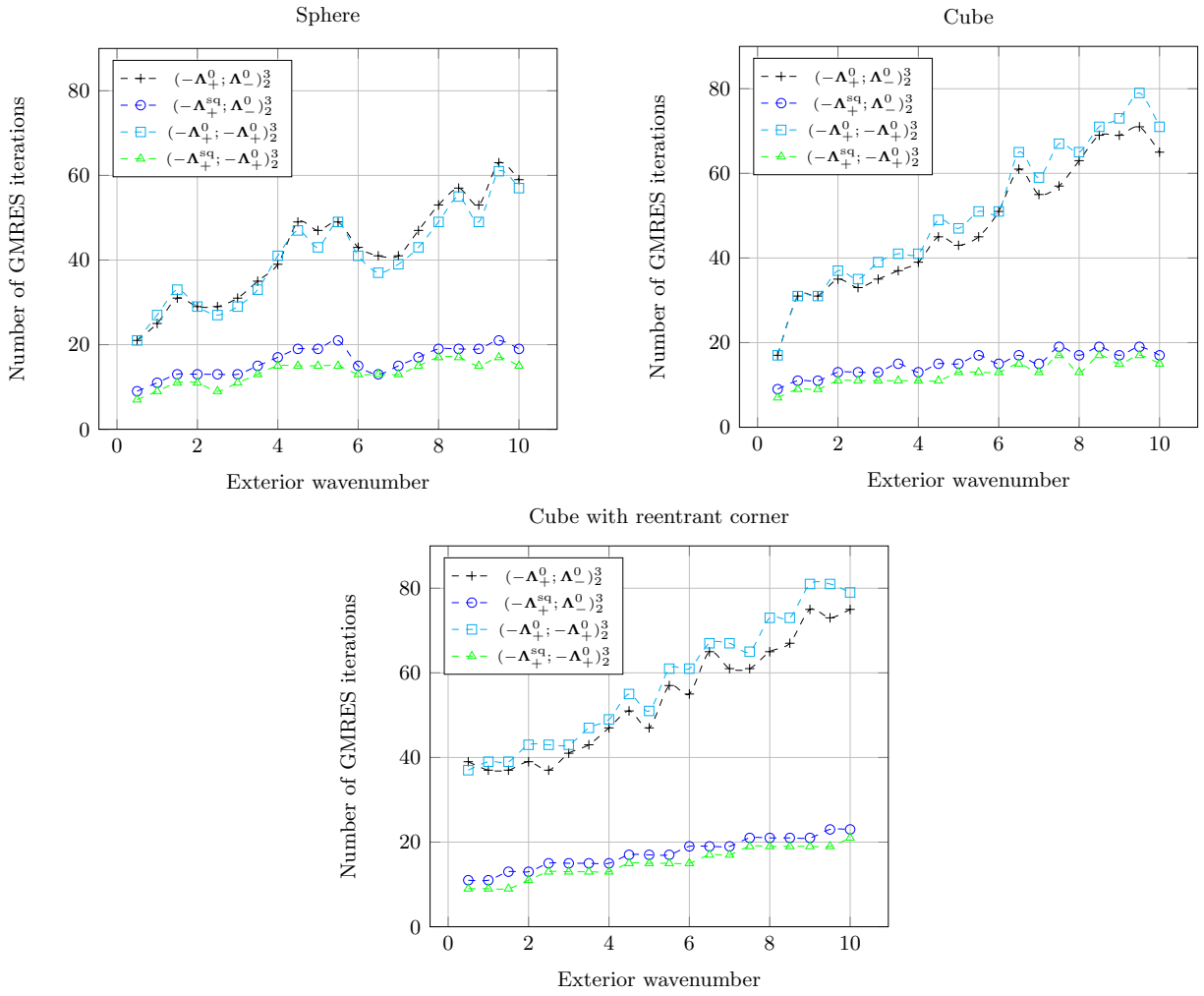

Figure 7: Number of GMRES iterations for the weak FEM-BEM coupling vs the exterior wavenumber k_+ (with $k_- = 2k_+$, $\mathcal{Z}_- = \mathcal{Z}_+/2$, $n_\lambda = 5$).

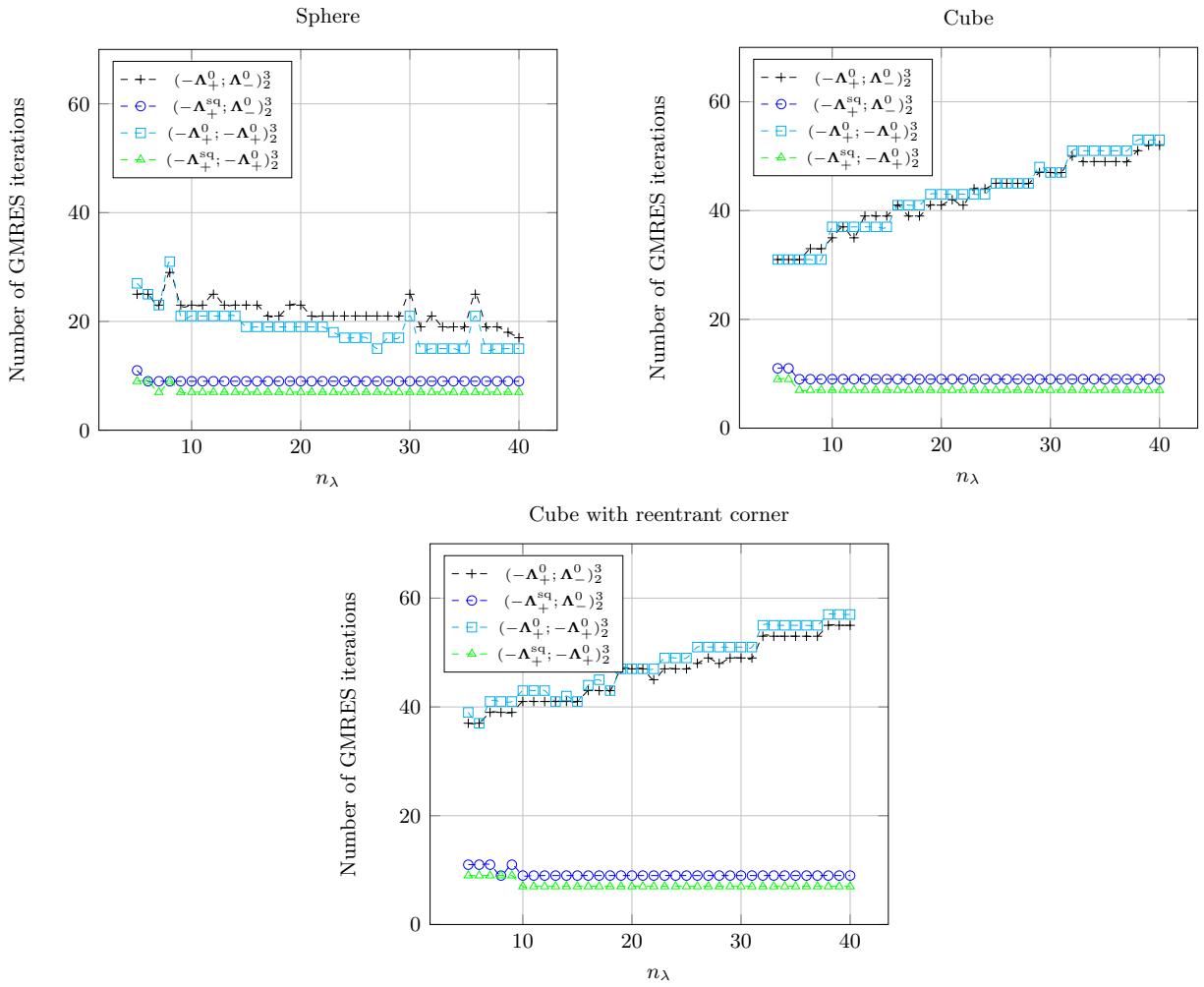

Figure 8: Number of GMRES iterations for the weak FEM-BEM coupling vs the discretization density n_λ (with $k_- = 2$, $k_+ = 1$, $\mathcal{Z}_- = \mathcal{Z}_+/2$).

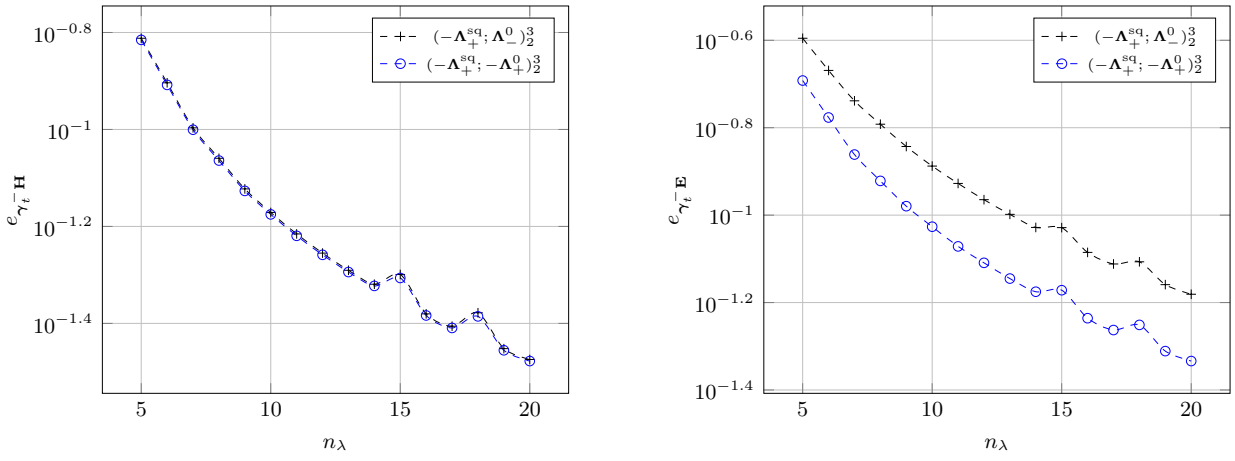

Figure 9: Relative errors between the analytical and numerical magnetic/electric surface currents as functions of the discretization density n_λ (with $k_- = 4$, $k_+ = 2$, $\mathcal{Z}_- = \mathcal{Z}_+/2$).

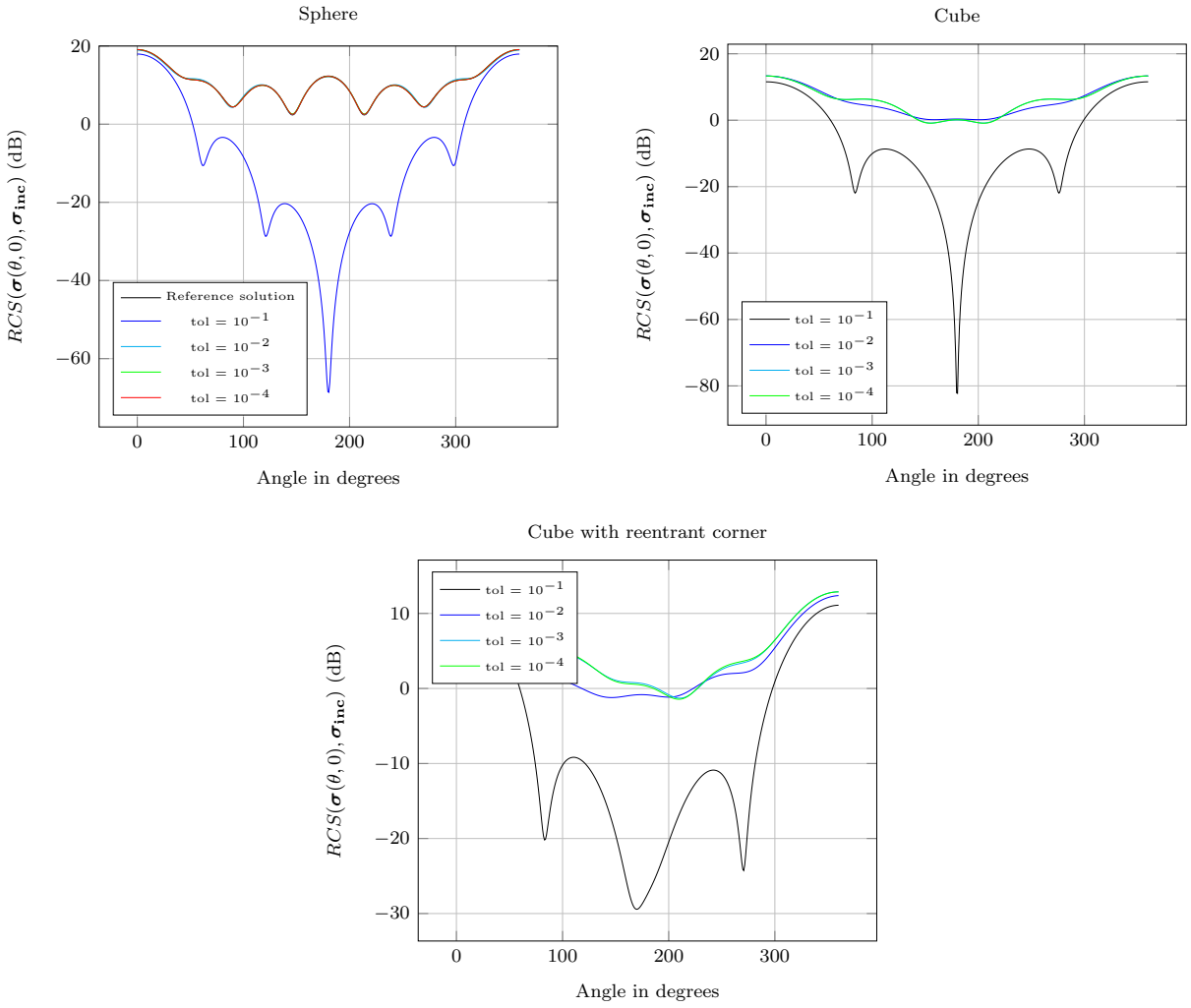

Figure 10: Convergence of the RCS with respect to the GMRES tolerance for the weak FEM-BEM coupling (with $k_- = 6$, $k_- = 3$, $\mathcal{Z}_- = \mathcal{Z}_+/2$, $n_\lambda = 10$).

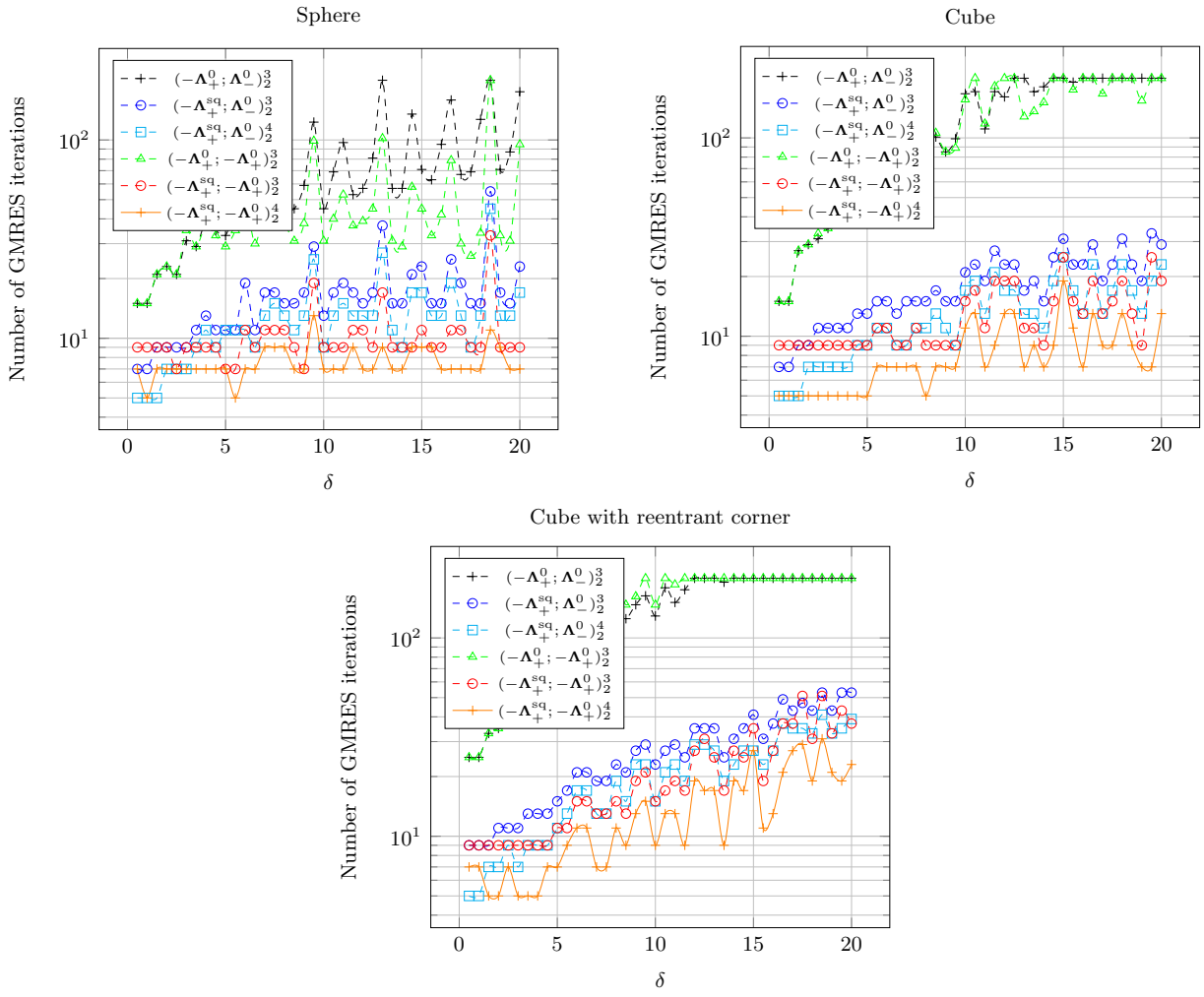

Figure 11: Number of GMRES iterations for the weak FEM-BEM coupling vs the contrast parameter δ (with $k_+ = 1$, $n_\lambda = 5$).

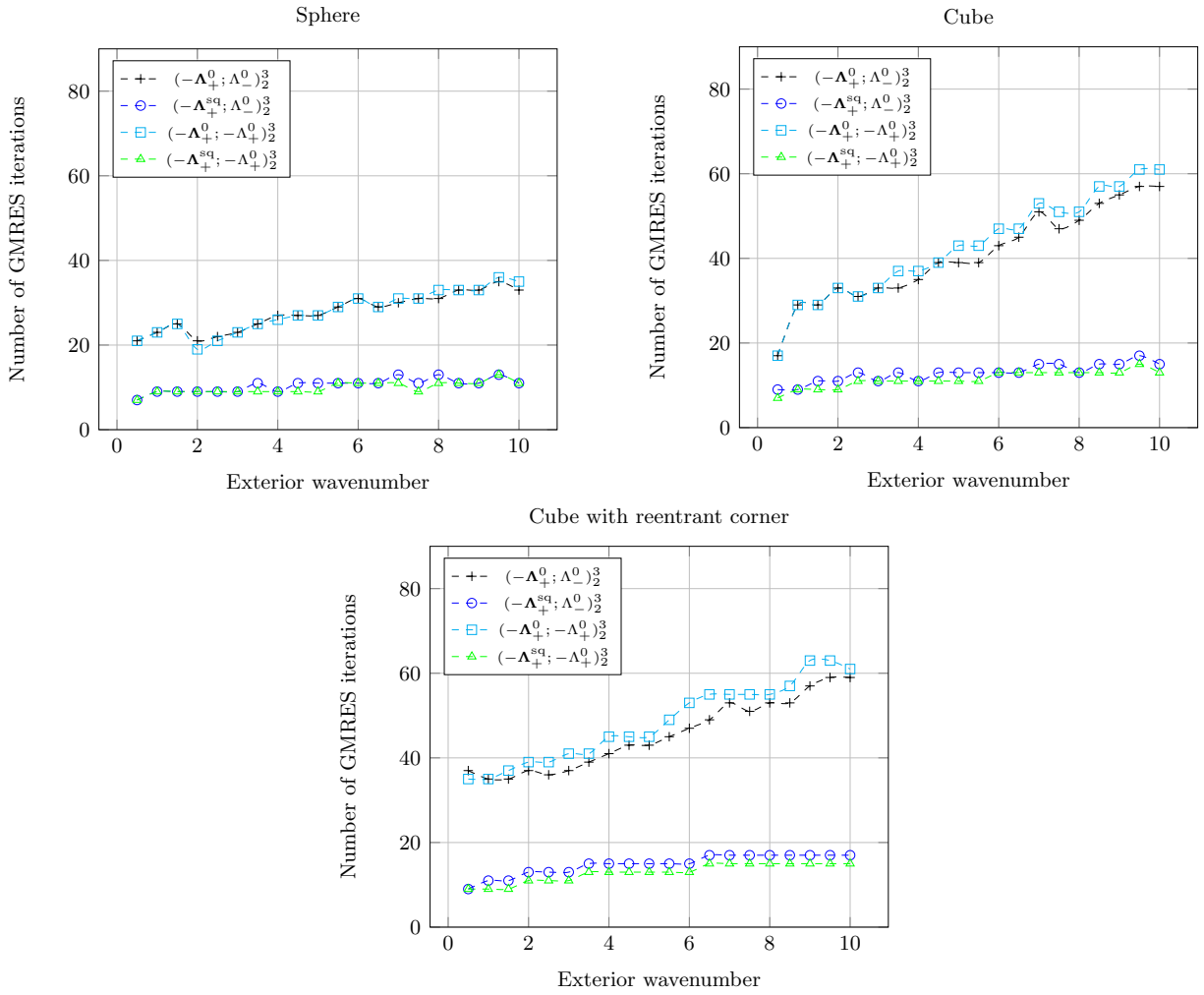

Figure 12: Number of GMRES iterations for the weak FEM-BEM coupling vs the exterior wavenumber k_+ (with $\delta = 2$, $n_\lambda = 5$).

Équipements de Calcul Intensif (CÉCI), funded by the Fonds de la Recherche Scientifique de Belgique (F.R.S.-FNRS) under Grant No. 2.5020.11 and by the Walloon Region.

References

[1] A. Alonso-Rodriguez and L. Gerardo-Giorda. New nonoverlapping domain decomposition methods for the harmonic Maxwell system. *SIAM Journal on Scientific Computing*, 28(1):102–122, 2006.

[2] A. Bachelot and V. Lange. Time dependent integral method for Maxwell's system with impedance boundary condition. *WIT Transactions on Modelling and Simulation*, 11, 1995.

[3] A. Bendali, Y. Boubendir, and M. B. Fares. A FETI-like domain decomposition method for coupling finite elements and boundary elements in large-size problems of acoustic scattering. *Computers & Structures*, 85(9):526–535, 2007.

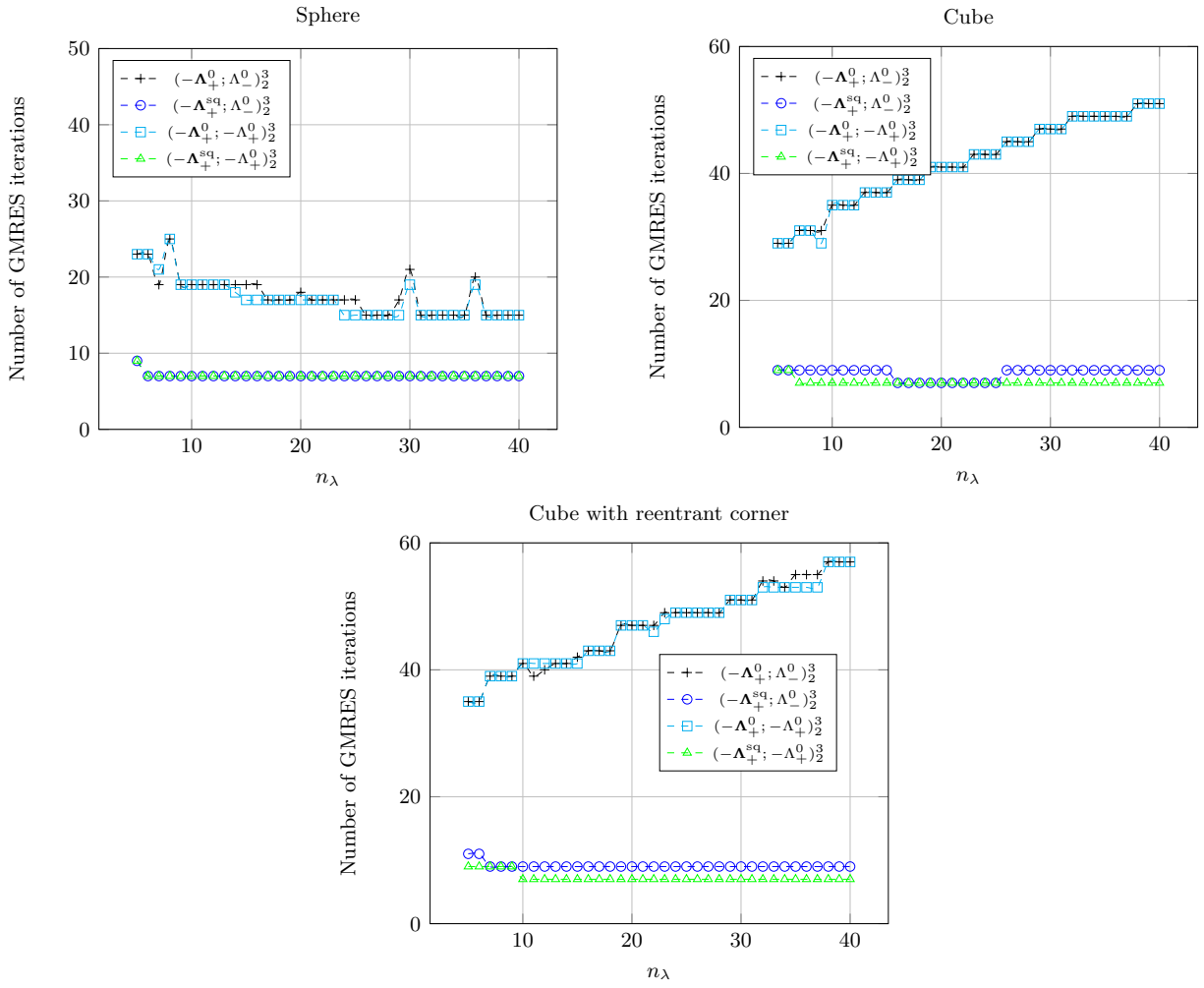

Figure 13: Number of GMRES iterations for the weak FEM-BEM coupling vs the discretization density n_λ (with $k_+ = 1$, $\delta = 2$).

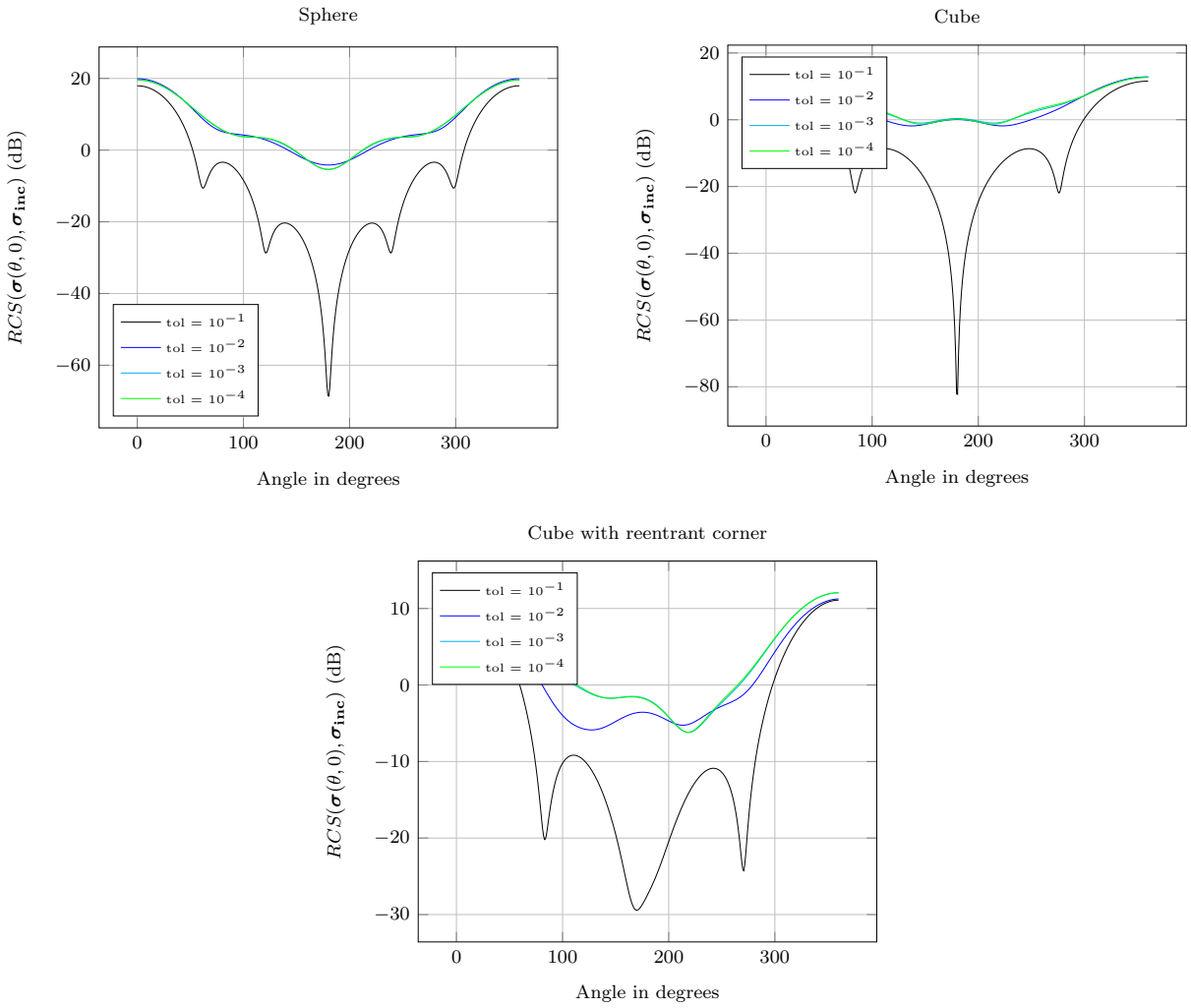

Figure 14: Convergence of the RCS with respect to the GMRES tolerance for the weak FEM-BEM coupling (with $k_- = 3$, $\delta = 2$, $n_\lambda = 10$).

[4] J.-P. Bérenger. A perfectly matched layer for the absorption of electromagnetic waves. *Journal of Computational Physics*, 114(2):185–200, 1994.

[5] M. Born and E. Wolf. *Principle of Optics: Electromagnetic Theory of Propagation, Interference and Diffraction of Light*. Pergamon Press, 2013.

[6] Y. Boubendir, A. Bendali, and M. B. Fares. Coupling of a non-overlapping domain decomposition method for a nodal finite element method with a boundary element method. *International Journal for Numerical Methods in Engineering*, 73(11):1624–1650, 2008.

[7] S. Börm. *Efficient Numerical Methods for Nonlocal Operators: H2-matrix Compression, Algorithms and Analysis*, volume 14. European Mathematical Society, 2010.

[8] B. Caudron. *Couplages FEM-BEM faibles et optimisés pour des problémes de diffraction*

harmoniques en acoustique et en électromagnétisme. PhD thesis, Université de Lorraine, France and Université de Liège, Belgique, 2018.

[9] B. Caudron, X. Antoine, and C. Geuzaine. Optimized weak coupling of boundary element and finite element methods for acoustic scattering. *Journal of Computational Physics*, 421(3):109737, 2020.

[10] W. Chew and W. Weedon. A 3D perfectly matched medium from modified Maxwell's equations with stretched coordinates. *Microwave and Optical Technology Letters*, 7(13):599–604, 1994.

[11] D. Colton and R. Kress. *Integral Equation Methods in Scattering Theory*. SIAM, 2013.

[12] A. de La Bourdonnaye. Some formulations coupling finite element and integral equation methods for Helmholtz equation and electromagnetism. *Numerische Mathematik*, 69(3):257–268, 1995.

[13] B. Després, P. Joly, and J. E. Roberts. A domain decomposition method for the harmonic Maxwell equations. In *Iterative methods in linear algebra*, pages 475–484, 1991.

[14] V. Dolean, M. J. Gander, and L. Gerardo-Giorda. Optimized Schwarz methods for Maxwell's equations. *SIAM Journal on Scientific Computing*, 31(3):2193–2213, 2009.

[15] M. El Bouajaji, X. Antoine, and C. Geuzaine. Approximate local magnetic-to-electric surface operators for time-harmonic Maxwell's equations. *Journal of Computational Physics*, 279:241–260, 2014.

[16] M. El Bouajaji, V. Dolean, M.J. Gander, and S. Lanteri. Optimized schwarz methods for the time-harmonic Maxwell equations with damping. *SIAM Journal on Scientific Computing*, 34(4):A2048–A2071, 2012.

[17] M. El Bouajaji, B. Thierry, X. Antoine, and C. Geuzaine. A quasi-optimal domain decomposition algorithm for the time-harmonic Maxwell's equations. *Journal of Computational Physics*, 294:38–57, 2015.

[18] O. G. Ernst and M. J. Gander. *Why it is Difficult to Solve Helmholtz Problems with Classical Iterative Methods*, pages 325–363. Springer Berlin Heidelberg, Berlin, Heidelberg, 2012.

[19] C. Geuzaine and J.-F. Remacle. Gmsh: a three-dimensional finite element mesh generator with built-in pre- and post-processing facilities. *International Journal for Numerical Methods in Engineering*, 79(11):1309–1331, 2009.

[20] W. Hackbusch. *Hierarchical Matrices: Algorithms and Analysis*, volume 49. Springer, 2015.

[21] R. Hiptmair. Coupling of finite elements and boundary elements in electromagnetic scattering. *SIAM Journal on Numerical Analysis*, 41(3):919–944, 2003.

[22] R. Hiptmair and P. Meury. Stabilized FEM–BEM coupling for Maxwell transmission problems. In *Modeling and Computations in Electromagnetics*, pages 1–38. Springer Berlin Heidelberg, 2008.

[23] J.-M. Jin. *The Finite Element Method in Electromagnetics*. John Wiley & Sons, 3rd edition, 2015.

[24] V. Levillain. *Couplage éléments finis-équations intégrales pour la résolution des équations de Maxwell en milieu hétérogène*. PhD thesis, Ecole Polytechnique, 1991.

[25] J. Liu and J.M. Jin. A highly effective preconditioner for solving the finite element-boundary integral matrix equation of 3-D scattering. *IEEE Transactions on Antennas and Propagation*, 50(9):1212–1221, 2002.

[26] Y. Liu. *Fast Multipole Boundary Element Method: Theory and Applications in Engineering*. Cambridge University Press, 2009.

[27] Ph. Marchner, X. Antoine, C. Geuzaine, and H. Bériot. Construction and numerical assessment of local absorbing boundary conditions for heterogeneous time-harmonic acoustic problems. *Preprint HAL-03196015, submitted*, 2021.

[28] F. A. Milinazzo, C. A. Zala, and G. H. Brooke. Rational square-root approximations for parabolic equation algorithms. *The Journal of the Acoustical Society of America*, 101(2):760–766, 1997.

[29] Axel Modave, Christophe Geuzaine, and Xavier Antoine. Corner treatments for high-order local absorbing boundary conditions in high-frequency acoustic scattering. *Journal of Computational Physics*, 401:109029, 2020.

[30] P.B. Monk and A.K. Parrott. A dispersion analysis of finite element methods for Maxwell's equations. *SIAM Journal on Scientific Computing*, 15(4):916–937, 1994.

[31] J.-C. Nédélec. *Acoustic and Electromagnetic Equations: Integral Representations for Harmonic Problems*, volume 144. Springer-Verlag, 2001.

[32] Z. Peng and J.-F. Lee. Non-conformal domain decomposition method with second-order transmission conditions for time-harmonic electromagnetics. *Journal of Computational Physics*, 229(16):5615–5629, 2010.

[33] Z. Peng, V. Rawat, and J.-F. Lee. One way domain decomposition method with second order transmission conditions for solving electromagnetic wave problems. *Journal of Computational Physics*, 229(4):1181–1197, 2010.

[34] P. A. Raviart and J. M. Thomas. A mixed finite element method for 2-nd order elliptic problems. In *Mathematical Aspects of Finite Element Methods*, page 292–315. Springer, 1977.

[35] V. Rawat and J.-F. Lee. Nonoverlapping domain decomposition with second order transmission condition for the time-harmonic Maxwell's equations. *SIAM Journal on Scientific Computing*, 32(6):3584–3603, 2010.

[36] A. Royer, E. Béchet, and C. Geuzaine. Gmsh-Fem: an efficient finite element library based on Gmsh, 14th World Congress on Computational Mechanics (WCCM) & ECCOMAS Congress, 2021.

[37] Y. Saad. *Iterative Methods for Sparse Linear systems*. SIAM, 2003.

[38] Y. Saad and M.H. Schultz. GMRES: A Generalized Minimal Residual algorithm for solving nonsymmetric linear systems. *SIAM Journal on Scientific and Statistical Computing*, 7(3):856–869, 1986.

[39] M. W. Scroggs, T. Betcke, E. Burman, W. Śmigaj, and E. van 't Wout. Software frameworks for integral equations in electromagnetic scattering based on Calderón identities. *Computers and Mathematics with Applications*, 74(11):2897–2914, 2017.

[40] X.-Q. Sheng, J.-M. Jin, J. Song, C.-C. Lu, and W. C. Chew. On the formulation of hybrid finite element and boundary-integral methods for 3-D scattering. *IEEE Transactions on Antennas and Propagation*, 46(3):303–311, 1998.

[41] B. Stupfel and M. Chanaud. High-order transmission conditions in a domain decomposition method for the time-harmonic Maxwell's equations in inhomogeneous media. *Journal of Computational Physics*, 372:385–405, 2018.

[42] P. Šolín, K. Segeth, and I. Doležel. *Higher-order Finite Element Methods*. Chapman & Hall/CRC, 2003.

[43] M. Vouvakis, K. Zhao, S.-M. Seo, and J.-F. Lee. A domain decomposition approach for non-conformal couplings between finite and boundary elements for unbounded electromagnetic problems in $\mathbb{R}^3$. *Journal of Computational Physics*, 225(1):975–994, 2007.

[44] X. Yuan. Three-dimensional electromagnetic scattering from inhomogeneous objects by the hybrid moment and finite element method. *IEEE Transactions on Microwave Theory and Techniques*, 38(8):1053–1058, 1990.